Research Paper

Network pharmacology and experimental evaluation strategies to decipher the underlying pharmacological mechanism of Traditional Chinese Medicine CFF-1 against prostate cancer

Yong Wei[1,*], Mingxia Zhu[2,*], Ye Chen[3,*], Qianying Ji[4], Jun Wang[4], Luming Shen[1], Xin Yang[1], Haibin Hu[1], Xin Zhou[5,6], Qingyi Zhu[1]

[1]Department of Urology, The Second Affiliated Hospital of Nanjing Medical University, Nanjing 210000, China
[2]Department of Radiation Oncology, The First Affiliated Hospital of Soochow University, Suzhou 215006, China
[3]The First Medicine College, Taizhou Campus of Nanjing University of Traditional Chinese Medicine, Taizhou 225300, China
[4]Department of Urology, Jiangsu Province Hospital of Chinese Medicine, Affiliated Hospital of Nanjing University of Chinese Medicine, Nanjing 210029, China
[5]Department of Oncology, The Affiliated Suqian First People's Hospital of Nanjing Medical University, Suqian 223812, China
[6]Department of Oncology, The First Affiliated Hospital of Nanjing Medical University, Nanjing 210029, China
[*]Equal contribution

Correspondence to: Qingyi Zhu, Xin Zhou, Haibin Hu; **email:** drzhuqingy@126.com, https://orcid.org/0000-0002-0965-4700; zhouxin5523@jsph.org.cn, hob_002@163.com, https://orcid.org/0009-0005-1335-2704
Keywords: prostate cancer, Traditional Chinese Medicine, CFF-1, network pharmacology, prognosis
Received: August 3, 2023 **Accepted:** February 20, 2024 **Published:** March 13, 2024

ABSTRACT

Prostate cancer (PCa) is a common malignancy in elderly men. We have applied Traditional Chinese Medicine CFF-1 in clinical treatments for PCa for several years. Here, we aimed to identify the underlying mechanism of CFF-1 on PCa using network pharmacology and experimental validation. Active ingredients, potential targets of CFF-1 were acquired from the public databases. Subsequently, protein-protein interaction (PPI) and the herbs-active ingredients-target network was constructed. A prognostic model for PCa was also constructed based on key targets. *In vitro* experiments using PCa cell lines CWR22Rv1 and PC-3 were carried out to validate the potential mechanism of CFF-1 on PCa. A total of 112 bioactive compounds and 359 key targets were screened from public databases. PPI and herbs-active ingredients-target network analysis determined 12 genes as the main targets of CFF-1 on PCa. Molecular docking studies indicated that the primary active ingredients of CFF-1 possess strong binding affinity to the top five hub targets. DNMT3B, RXRB and HPRT1 were found to be involved in immune regulation of PCa. *In vitro*, CFF-1 was found to inhibit PCa cell proliferation, migration, invasion and induce apoptosis via PI3K-Akt, HIF-1, TNF, EGFR-TKI resistance and PD-1 checkpoint signaling pathways. This study comprehensively elucidates the underlying molecular mechanism of CFF-1 against PCa, offering a strong rationale for clinical application of CFF-1 in PCa treatment.

INTRODUCTION

Prostate cancer (PCa) ranks as the second deadly malignancy among men worldwide [1]. While early diagnosis, surgery and radiotherapy have enhanced survival rates in patients with PCa, therapeutic options for advanced stages, especially castration-resistant prostate cancer (CRPC), remain constrained [2–4].

Network pharmacology, a bioinformatics method, facilitates the enhancement of drug efficacy, minimization of adverse reactions, and development of new drugs by analyzing complex compositions and disease-related signaling pathways. It has also been instrumental in deciphering the intricate interplay between active components of natural products, diseases, and targets [5, 6].

Traditional Chinese Medicine (TCM), acting on multiple targets rather than a single target, is more systematic in treating corresponding diseases [7]. The efficacy of TCM lies in the synergistic effect of multiple targets and components, regulating diverse biological mechanisms. However, the action mechanism of TCM formulas, with their intricate components, is more complex than that of single medicines [8–10]. Traditional pharmacological studies of TCM, often focused on individual ingredients or medicines, struggle to elucidate the synergistic effects of various chemical constituents.

CFF-1, a TCM obtained from Fusong Xu, a renowned TCM practitioner from Jiangsu Province Hospital of Chinese Medicine, has been employed in clinical settings to treat PCa for several years. According to our previous reports, CFF-1 suppressed cell growth and promoted apoptosis through EGFR-related pathways in PCa [11]. It is also reported to counteract PCa through suppressing PD-1/PD-L1 checkpoint signaling via EGFR-related pathways [12]. Nevertheless, the comprehensive mechanism of CFF-1 in treating PCa has yet to be fully elucidated using robust methodologies. Network pharmacology, merging the advantages of TCM with the most advanced medical technology, has become a favorable approach for TCM research [13, 14].

We utilized a comprehensive network pharmacology and molecular docking approach to investigate the bioactives of CFF-1, predict their effective targets, and understand the underlying molecular mechanisms in PCa. A prognostic model based on key targets was also constructed. Finally, we verified the predicted results in PCa cell lines.

RESULTS

Active compounds in CFF-1 and target screening of CFF-1 on PCa

Initially, 78 active compounds in CFF-1, each with OB ≥30% and DL ≥0.1 in CFF-1, were collected from TCMSP platform. Subsequently, 70 active compounds with $p < 0.05$, score >20 were obtained from BATMAN-TCM platform. After integrating these findings, 112 active compounds were selected for further study (Table 1). The targets for the candidate compounds in CFF-1 were explored from TCMSP and BATMAN-TCM, identifying 131 and 848 putative targets, respectively. There were 41 overlapping targets among the two sets. Ultimately, 938 targets for CFF-1 active components were acquired by integrating the overlapping targets (Figure 1A). Additionally, 2682 target genes related to PCa were acquired from the Genecards by setting the correlation score >20 and 495 target genes were acquired from OMIM databases. A total of 3022 target genes acquired from the two sets after eliminating the overlaps (Figure 1B). Nine hundred and thirty-eight targets for drug active components and 3022 targets for PCa were screened out by Perl language program and R language software. In total, 359 overlapping target genes were recognized as key targets related to both CFF-1 and PCa for further analyses (Figure 1C).

Compound-target network and analysis

Upon entering the above 359 key targets into STRING, we obtained a key targets PPI network of CFF-1 on PCa. Subsequent analysis of this PPI network focused on "degree" was applied to select the target in the core position (Figure 2A). The top 30 target genes with high degree were shown in Figure 2B. The 53 core targets were further screened by setting interaction score ≥0.9 and degree ≥20. Cytoscape software was applied to construct the herbs-active ingredients-target network, containing 112 nodes (55 for candidate active ingredients and 53 for core targets) and 253 edges. In the network, the nodes with more edges might play essential roles in the pharmacological processes, and 12 nodes (edge ≥5) were determined as the main targets of CFF-1 on PCa for further analysis, including NCOA2, RXRA, ESR1, NCOA1, PPARG, IL1B, TNF, IKBKB, NR3C1, IL4, IL6 and PRKCA (Figure 2C).

Molecular docking verification

As previously mentioned, PIK3R1, AKT1, MAPK1, MAPK3 and SRC were the top five hub targets in PPI network. These targets were then docked with their respective active ingredients. The ligand-receptor binding energy values, indicative of binding stability, were presented in Figure 3A. Generally, a binding energy lower than −5 kcal/mol is considered indicative of stable binding. Notably, coryneine establishes two hydrogen bonds with GLU-17 and THR-18 in PIK3R1, while baicalein forms three hydrogen bonds with GLU-91, HIS-89 and HIS-13 in AKT1. Diosgenin forms one hydrogen bond with GLY-16 in AKT1. Coryneine and digitalis glycoside bound to MAPK1 with binding energy values of −5.6 kcal/mol and −9 kcal/mol, respectively.

Table 1. Active compounds in CFF-1.

Number	Active compounds	Number	Active compounds	Number	Active compounds
1	Isoliquiritigenin	2	DFV	3	baicalein
4	3′-Methoxydaidzein	5	beta-sitosterol	6	sitosterol
7	(Z)-1-(2,4-dihydroxyphenyl)-3-(4-hydroxyphenyl)prop-2-en-1-one	8	(2R)-7-hydroxy-2-(4-hydroxyphenyl)chroman-4-one	9	1H-Cycloprop(e)azulen-7-ol, decahydro-1,1,7-trimethyl-4-methylene-,(1aR-(1aalpha, 4aalpha,7beta,7abeta,7balpha))
10	4′,5-Dihydroxyflavone	11	2-Acridinecarboxylic acid	12	(Z)-nonadec-6-enoic acid
13	Azetidine-2-Carboxylic Acid	14	Aspartic Acid	15	Digitalis Glycoside
16	Homoserine	17	Mannose	18	EIC
19	Aeginetic acid	20	jioglutin D	21	METHYL PALMITOLEATE
22	Stigmasterol	23	Uridine	24	DMEP
25	1,2-Dibenzoylethane	26	WLN: RVO2R	27	(−)-taxifolin
28	ELD	29	diosgenin	30	()-alpha-Longipinene
31	(+)-catechin	32	(−)-Caryophyllene oxide	33	(−)-alpha-cedrene
34	DBP	35	ent-Epicatechin	36	alpha-Longipinene
37	DIBP	38	()-Aromadendrene	39	beta-Cubebene
40	(−)-Epoxycaryophyllene	41	oleic acid	42	Hepanal
43	58870_FLUKA	44	()-alpha-Funebrene	45	phytol
46	8-Deoxy-14-Dehydro-Aconosine	47	1,2-Benzenedicarboxylicacid, mono(2-ethyl) hexylester	48	(−)-Alloaromadendrene
49	Procurcumenol	50	Tetradecanal	51	Cinnamaldehyde
52	5-Cinnamoyl-9-O-Acetylphototaxicin I	53	Anethole	54	Protocatechuic Acid
55	Coumarinic Acid	56	Gamma-Sitosterol	57	Camphor
58	Melilotocarpan A	59	Farnesol	60	Nerolidol
61	Trans-Cinnamic Acid	62	Styrene	63	11,14-eicosadienoic acid
64	Delphin_qt	65	Deltoin	66	Deoxyandrographolide
67	Karanjin	68	Talatisamine	69	Benzoylaconine
70	Aconitine	71	Delgrandine	72	Aconine
73	14-Deoxy-11,12-Didehydroandrographolide	74	Deltaline	75	Delavaconitine
76	Deltamine	77	Carmichaeline	78	Delsoline
79	Salsolinol	80	Crassicauline A	81	Delphamine
82	Bullatine B	83	Benzoylhypaconine	84	Bullatine C
85	Coryneine	86	Vilmorrianine C	87	3-Acetylaconitine
88	Deoxyaconitine	89	Delphatine	90	M-Aminophenol
91	Karakoline	92	Hypaconitine	93	Talatizamine
94	Neojiangyouaconitine	95	Ignavine	96	Ortho-Aminophenol
97	Para-Aminophenol	98	Neokadsuranic Acid B	99	Benzoylmesaconine
100	taxifolin	101	Delbrusine	102	Mescaline
103	Higenamine	104	Carnosifloside I	105	Mesaconitine
106	Isotalatizidine	107	Neoline	108	P-Aminophenol
109	Delcorine	110	Delbrusine	111	Karacoline
112	Delbruline				

Among these, the binding affinity of digitalis glycoside to MAPK3 was the strongest, with a value of −12.9 kcal/mol. Additionally, nerolidol forms one hydrogen bond with GLU40 in SRC (Figure 3B–3H).

Enrichment analysis

To ascertain the involved pathways of CFF-1 on PCa, we carried out KEGG pathway analysis of 359 key targets. A total of 172 involved pathways were identified (Supplementary Table 1). Figure 4A displayed the top 20 enriched pathways, suggesting that the anti-cancer effect of CFF-1 on PCa likely results from a relatively complex and multi-pathway synergistic effect.

To further explore the biological role of involved targets of CFF-1 against PCa, the GO process analysis of 359 key targets was performed. A total of 238 GO terms were found (Supplementary Table 2). Figure 4B displayed the top 20 enriched terms related to PCa, suggesting that CFF-1 may exhibit its therapeutic effects through the above biological processes.

Prognostic model construction based on key targets

A total of 359 key target genes were subjected to LASSO regression analysis to identify genes for construction of risk score model for PCa patients in the TCGA database. The risk score for predicting DFS of each PCa patient was calculated as follows: Risk score = NFATC1 × 0.234 + ARG1 × 0.001 + DNMT3B × 0.315 − NR3C1 × 0.025 + RXRB × 0.105 + HPRT1 × 0.033 + SI × 0.037. A 7-gene signature was constructed. Patients were classified into high- and low-risk groups based on the median risk score (Figure 5A). A risk curve and a scatter plot were applied to show the risk score and the survival status of each PCa patient,

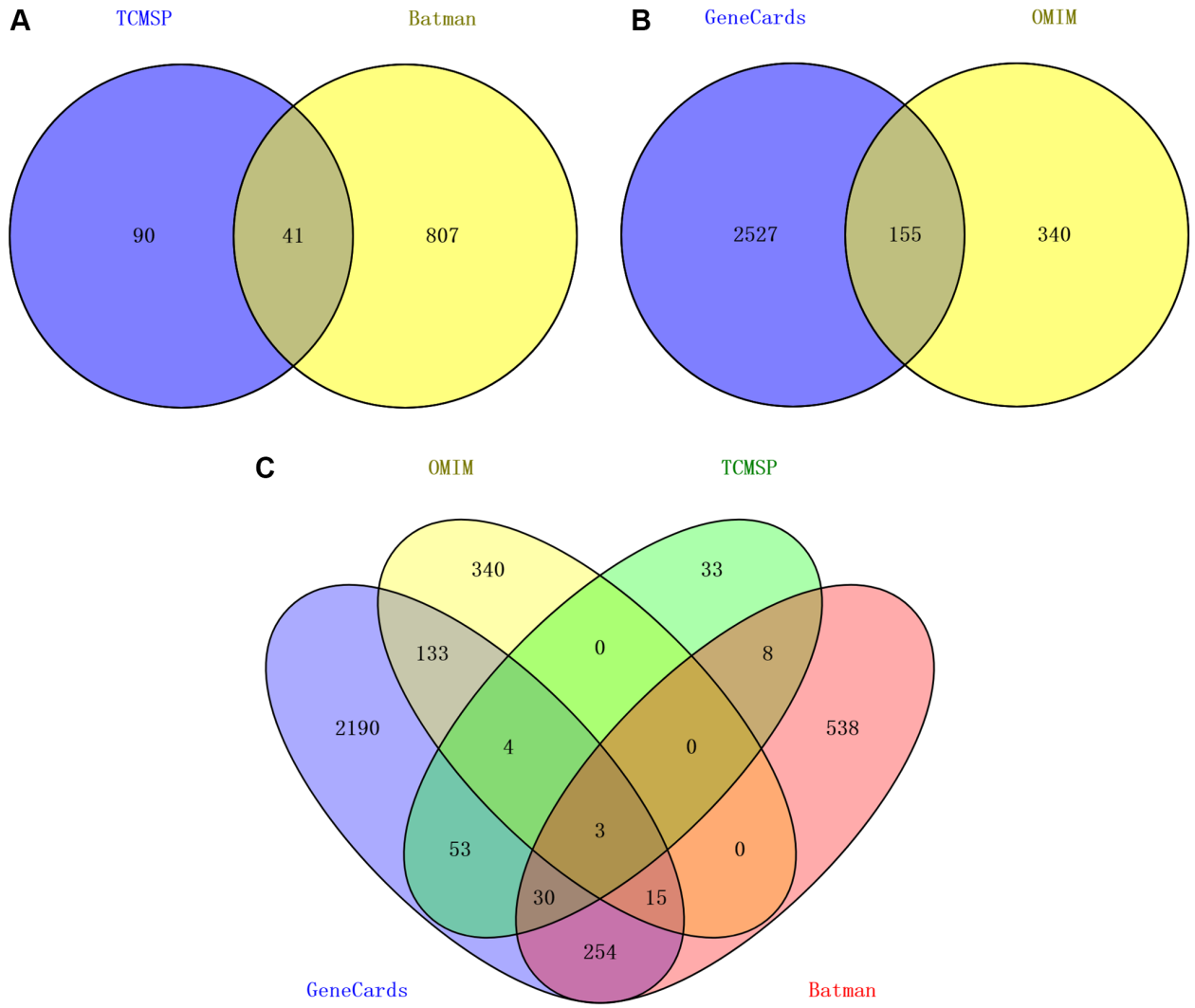

Figure 1. Target screening of CFF-1 on PCa. (**A**) Venn diagrams showing CFF-1 targets obtained from TCMSP and BATMAN-TCM. (**B**) Targets related to PCa acquired from Genecards and OMIM. (**C**) The intersection of targets for both CFF-1 and PCa.

respectively. Most recurrent cases were distributed in the high-risk group (Figure 5B). The expression profile of candidate genes indicated that NFATC1, ARG1, DNMT3B, NR3C1, RXRB, HPRT1 and SI were highly expressed in the high-risk group, except for NR3C1 (Figure 5C). PCa patients in the high-risk group had a significantly worse DFS than those in the low-risk group. AUC of ROC curve for the DFS prediction of risk score model was 0.867 (Figure 5D, 5E).

The risk score for predicting PFS was calculated as follows: Risk score =ALDOA × 0.0003 + DNMT3B × 0.222 + CSF2 × 0.099 + DNMT1 × 0.031 + EZH2 × 0.054 + ARRB2 × 0.019 − ESRRG × 0.025 + APOA2 ×

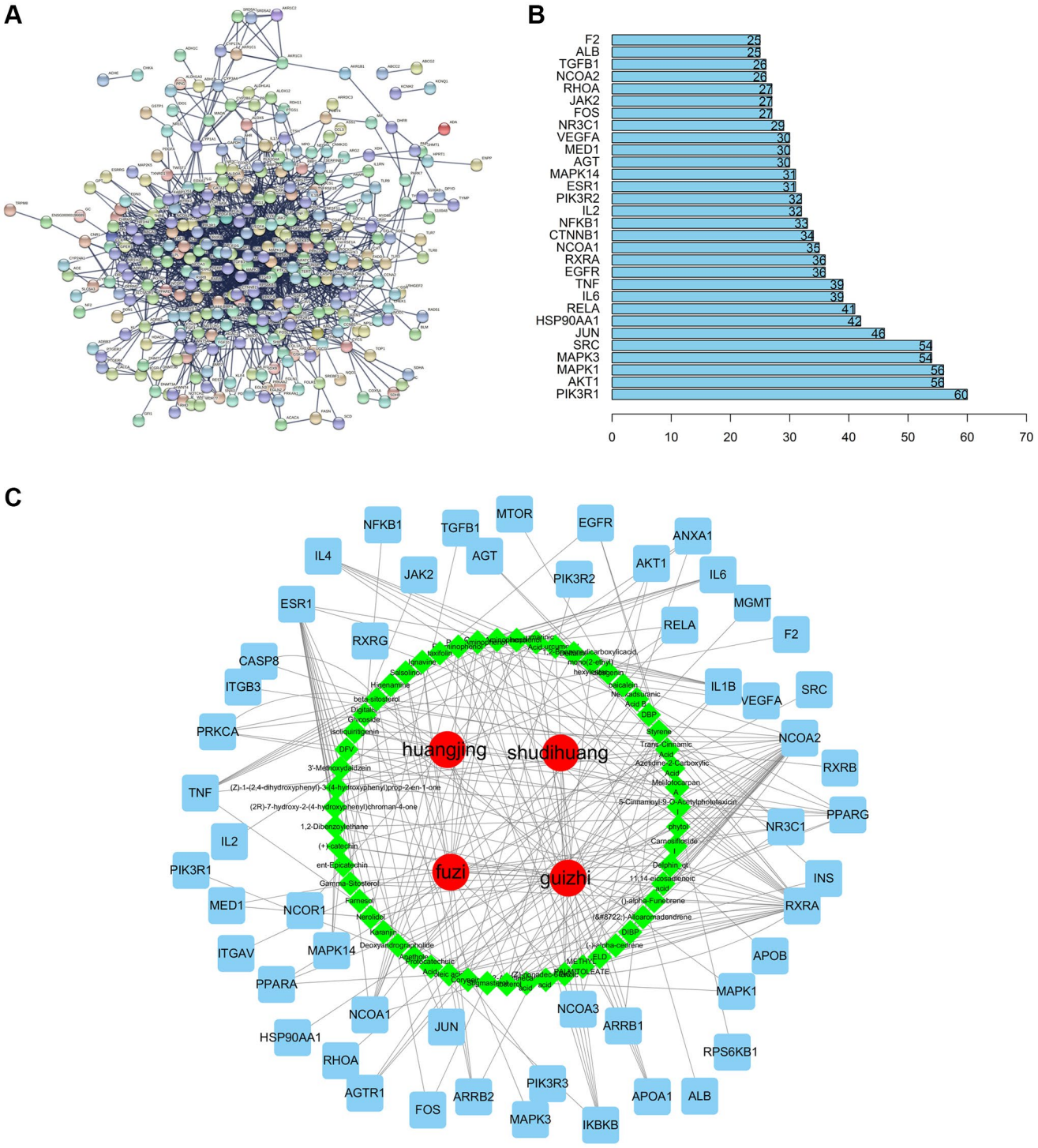

Figure 2. Compound-target network and analysis. (**A**) Key targets PPI network of CFF-1 on PCa. (**B**) Bar graph showing the top 30 targets with high degree. (**C**) The herbs-active ingredients-target network of CFF-1 on PCa.

0.007 + RXRB × 0.076 + HPRT1 × 0.021 − RDH11 × 0.0001. A 11-gene signature was constructed (Figure 5F). Progression patients were mainly distributed in the high-risk group (Figure 5G). The expression profile showed that ALDOA, DNMT3B, CSF2, DNMT1, EZH2, ARRB2, APOA2, RXRB and HPRT1 were highly expressed in the high-risk group, except for ESRRG and RDH11 (Figure 5H). Kaplan–Meier curves showed that PFS was significantly worse in high-risk patients than low-risk patients. AUC of ROC curve for the PFS prediction was 0.773 (Figure 5I, 5J).

For OS, though few patients reached the endpoint (10 of 495 patients), the risk score model was also constructed. The risk score for predicting OS was calculated as follows: Risk score = AR × 0.048 + AGTR1 × 0.062 + PPARD × 0.427 + PHB × 0.090 + RPS6KB1 × 0.620 + FADD × 0.821 − DNMT1 × 0.667 +AKR1C3 × 0.075. An 8-gene signature was constructed (Supplementary Figure 1A). More dead cases were found in the high-risk group (Supplementary Figure 1B). The heat map suggested that AR, AGTR1, PPARD, PHB, RPS6KB1, FADD, DNMT1 and AKR1C3 were overexpressed in the high-risk group, except for DNMT1 (Supplementary Figure 1C). Patients in the high-risk group had significantly shorter OS compared with those in the low-risk group. AUC of ROC curve for the OS prediction was 0.992 (Supplementary Figure 1D, 1E). Taken together, these gene signatures might effectively predict the prognosis of PCa and may act as potential targets for PCa therapy.

We then explored possible associations of risk scores with ESTIMATE score using the ESTIMATE algorithm. Using the CIBERSORT algorithm, the correlation between risk score and the infiltration of

A

Ligand	Receptor	PDB id	Binding energy (kcal/mol)
Coryneine	PIK3R1	1A0N	-4.8
baicalein	AKT1	1H10	-6.8
diosgenin	AKT1	1H10	-7.3
Coryneine	MAPK1	1PME	-5.6
Digitalis Glycoside	MAPK1	1PME	-9
Digitalis Glycoside	MAPK3	2ZOQ	-12.9
Nerolidol	SRC	1A07	-5.6

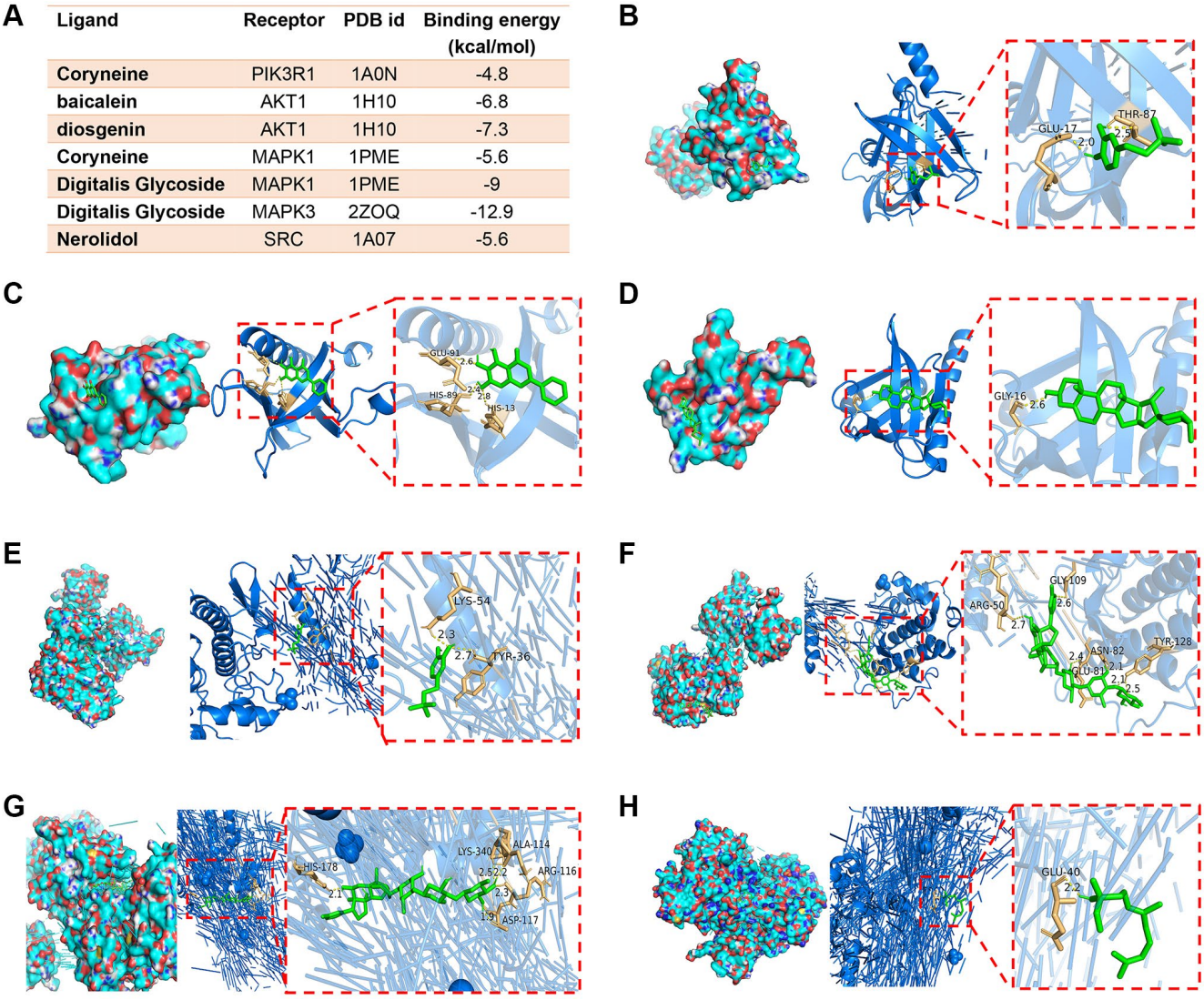

Figure 3. Representative images of molecular docking. (**A**) The results of ligand-receptor binding energy values. (**B**) Coryneine-PIK3R1. (**C**) Baicalein-AKT1. (**D**) Diosgenin-AKT1. (**E**) Coryneine-MAPK1. (**F**) Digitalis glycoside-MAPK1. (**G**) Digitalis glycoside-MAPK3. (**H**) Nerolidol-SRC.

22 immune cell subtypes were assessed. The risk score for predicting OS of PCa patient was negatively associated with stromal score, immune score, and ESTIMATE score, while positively with the infiltration of mast cells resting (Supplementary Figure 2A). The risk score for predicting DFS was negatively related to the infiltration of plasma cells, while positively Tregs and macrophages M2 (Supplementary Figure 2B). The risk score for predicting PFS was positively related to stromal score, immune score, ESTIMATE score, the infiltration of Tregs macrophages M1 and macrophages M2, while negatively with plasma cells and mast cells resting (Supplementary Figure 2C).

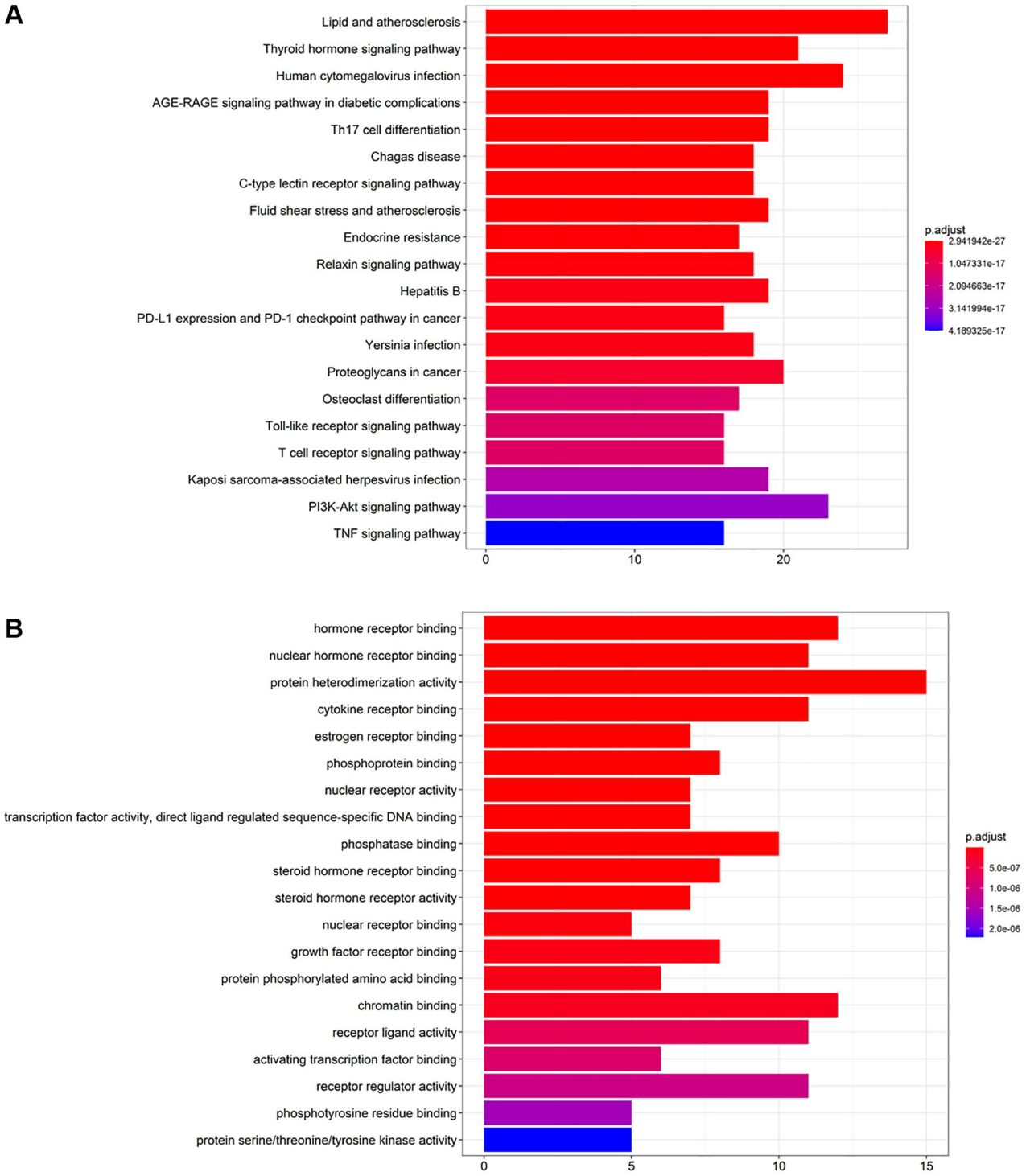

Figure 4. KEGG pathway enrichment and GO biological process analysis of key targets of CFF-1 on PCa. (**A**) The top 20 enriched pathways of KEGG pathway enrichment analysis. (**B**) The top 20 enriched terms of GO biological process analysis.

DNMT3B, RXRB and HPRT1 were the common target genes affecting both PFS and DFS in PCa patients. GO functional annotations and KEGG pathways enrichment were applied to evaluate the biological significance of DNMT3B, RXRB and HPRT1 in PCa. The results indicated that DNMT3B, RXRB and HPRT1 were widely involved in immune regulation (Supplementary Figure 3).

CFF-1 inhibited PCa cells proliferation and induced apoptosis

To evaluate the effect of CFF-1 on PCa as postulated from network pharmacology analysis, clonogenic assay, CCK8 and Edu assays were conducted in PC-3 cell line treated with different concentrations of CFF-1 (0, 2, 4, 6, 8 and 10 mg/ml). The cell colony formation efficiency of PC-3 cells was decreased dose dependently compared to the negative control (Figure 6A, 6C). Furthermore, a dose-dependent reduction in proliferation active cells was observed after 24 hours of CFF-1 treatment in the EdU assay (Figure 6B, 6D). The CCK8 assay confirmed a dose-dependent decrease in PCa cell viability (Figure 6E). In addition, CFF-1 treatment increased the percentage of apoptotic PC-3 cells dose dependently (Figure 7A–7H).

CFF-1 inhibited PCa cells migration and invasion

Subsequently, wound healing and transwell experiments were conducted to explore the migration and invasion abilities of PC-3 cells treated with CFF-1. We found that fewer cells migrated to the scratch site after 24 hours of CFF-1 treatment dose dependently (Figure 8A, 8C). Furthermore, the migration and invasion ability of PC-3 cells were significantly inhibited after treatment with increasing CFF-1 (Figure 8B, 8D, 8E).

CFF-1 attenuated proliferation pathways in PCa cells

According to network pharmacology analysis, the PI3K-Akt, HIF-1, TNF, EGFR-TKI resistance and PD-1

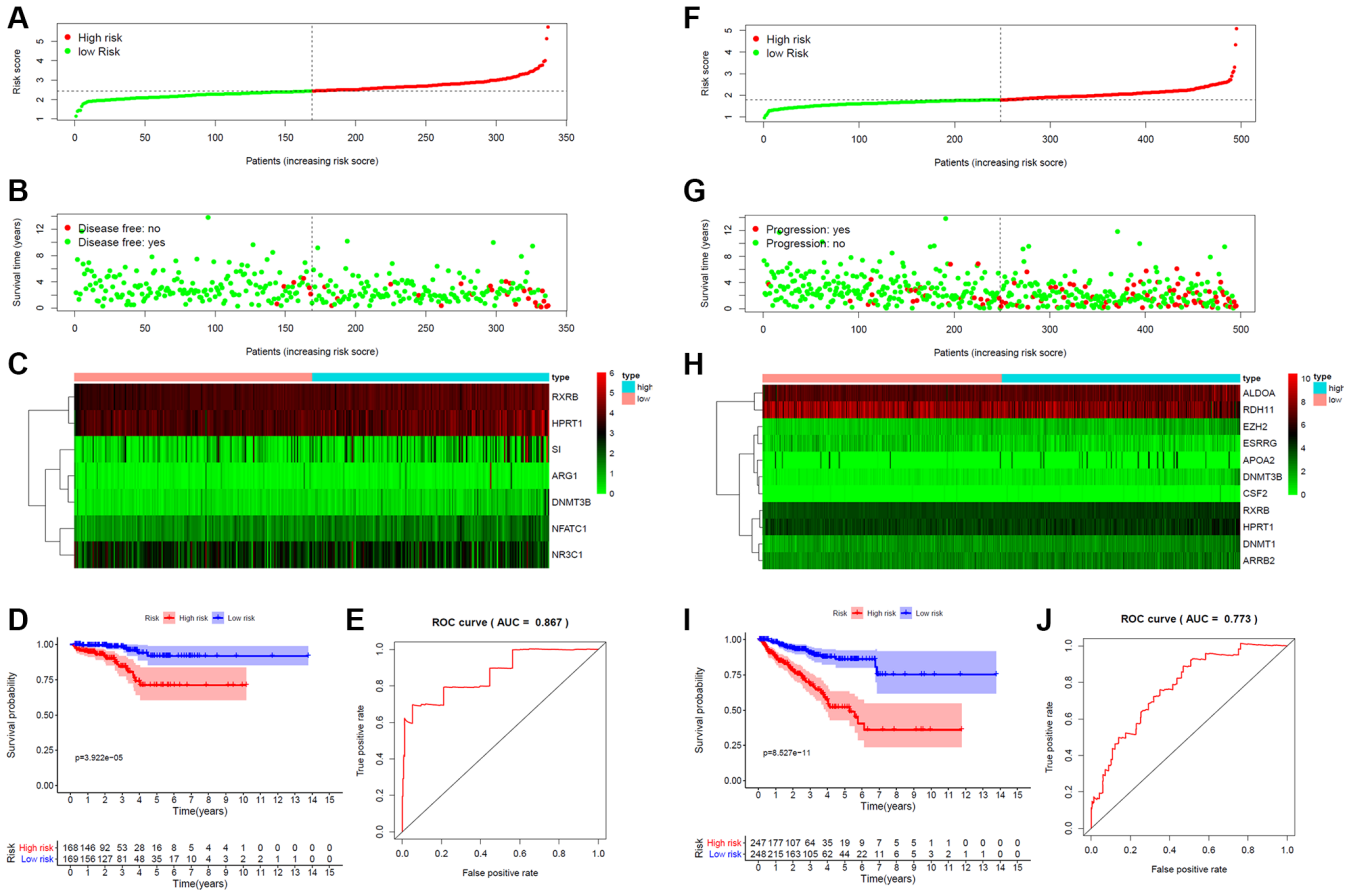

Figure 5. Risk score for target gene signature and outcome in PCa patients. (**A**) Risk score of a 7-gene signature for predicting DFS. (**B**) Disease status and duration of cases. (**C**) Heatmap of the 7 gene expression in PCa patients. (**D**) Kaplan-Meier curve for DFS in the low- and high-risk groups. (**E**) ROC curve for the DFS prediction of risk score model. (**F**) Risk score of a 11-gene signature for predicting PFS. (**G**) Progression status and duration of cases. (**H**) Heatmap of the 11 gene expression in PCa patients. (**I**) Kaplan-Meier curve for PFS in the low- and high-risk groups. (**J**) ROC curve for the PFS prediction of risk score model.

checkpoint pathway might play a crucial role in regulating PCa cell proliferation and survival by CFF-1. Then, we evaluated the expressions level of the common key targets of the five pathways. Pretreatment of CWR22Rv1 and PC3 cells with CFF-1 (2, 6 and 10 mg/ml) resulted in apparent repression of P-ERK1, NFκB1, RELA, P-mTOR, VEGFA, PD-L1, P-PI3K, P-AKT, TNF-α, P-EGFR and HIF-1α in dose dependently (Figure 9A, 9B). ELISA assays indicated that the secretory IL-6 of CWR22Rv1 and PC3 cells was blocked by CFF-1 dose dependently (Figure 9C, 9D). These findings suggested that the above five pathways might be crucial for CFF-1 anti-cancer effect in PCa.

DISCUSSION

In our previous study, the administration of CFF-1 in patients with metastatic castration-resistant prostate cancer (mCRPC) resulted in a significant reduction in Prostate-Specific Antigen (PSA) levels. This reduction is an important marker of CFF-1's therapeutic efficacy in slowing prostate cancer progression. Beyond this quantifiable impact on PSA levels, the study also recorded improvements in clinical symptoms associated with mCRPC. Patients undergoing CFF-1 treatment experienced alleviated symptoms, reflecting an improvement in their quality of life. Additionally, a notable decrease in fatigue was observed among patients receiving CFF-1. Our collective research has also shown that CFF-1 exerts potent anti-tumor immunity, effectively hindering tumor growth and metastasis in prostate cancer via the EGFR/JAK1/STAT3 pathway, subsequently inhibiting PD-1/PD-L1 checkpoint signaling. Additionally, CFF-1 promotes cell growth inhibition, autophagy, and apoptosis by targeting and inhibiting EGFR-related pathways in PCa [11–12]. Network pharmacology

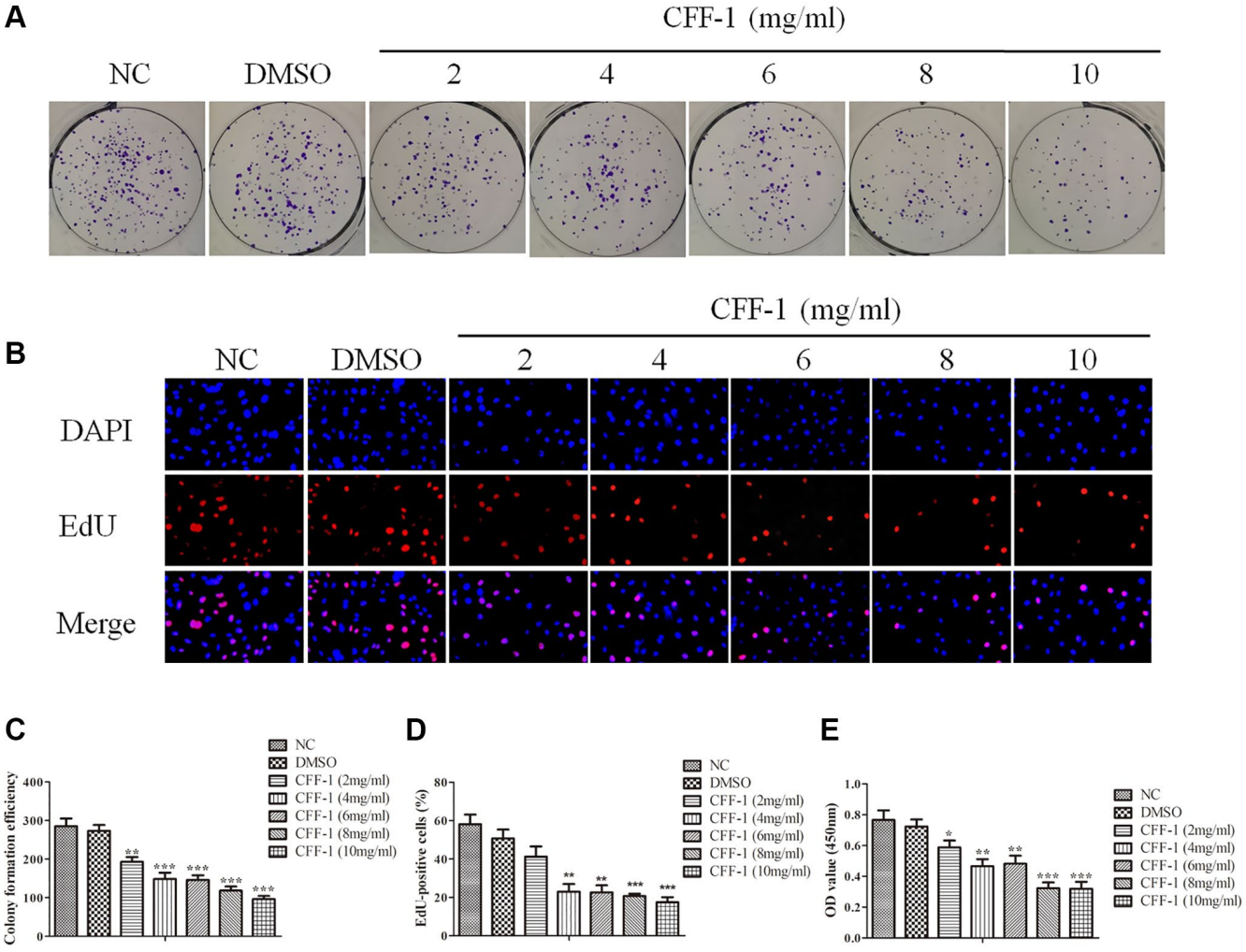

Figure 6. CFF-1 inhibited PCa cells proliferation. (**A**) The colony formation efficiency of PC-3 cell lines with varying concentrations of CFF-1 (mg/mL). (**B**) The EdU assay of proliferation active cells after 24 hours of CFF-1 treatment. (**C**) Quantification of the colony formation efficiency with bar graph. (**D**) Quantitative results of the EdU assay with bar graph. (**E**) The cell viability was determined by CCK8 assay after CFF-1 administration. $^{*}p < 0.05$, $^{**}p < 0.01$, $^{***}p < 0.001$.

combined with molecular docking have been used as a valuable tool to explore the complex mechanisms of TCM [5]. In this study, the role of CFF-1 was comprehensively elucidated through a multifaceted approach encompassing network pharmacology, bioinformatics, and *in vitro* validation. This approach, transcending traditional single-target strategies, aligns with the emerging paradigm shift in oncology towards multi-targeted therapies.

In our study, 112 bioactives and 359 key targets were screened, thus unveiling an extensive molecular framework for potential intervention in PCa. The herbs-active ingredients-target network demonstrated that NCOA2, RXRA, ESR1, NCOA1, PPARG, IL1B, TNF, IKBKB, NR3C1, IL4, IL6 and PRKCA could serve as main targets for CFF-1 on PCa. According to molecular docking results, the primary active ingredients exhibited a robust binding affinity to the top five hub targets, primarily through the formation of hydrogen bonds. This data not only enriches the current understanding of PCa but also opens new avenues for targeted therapy.

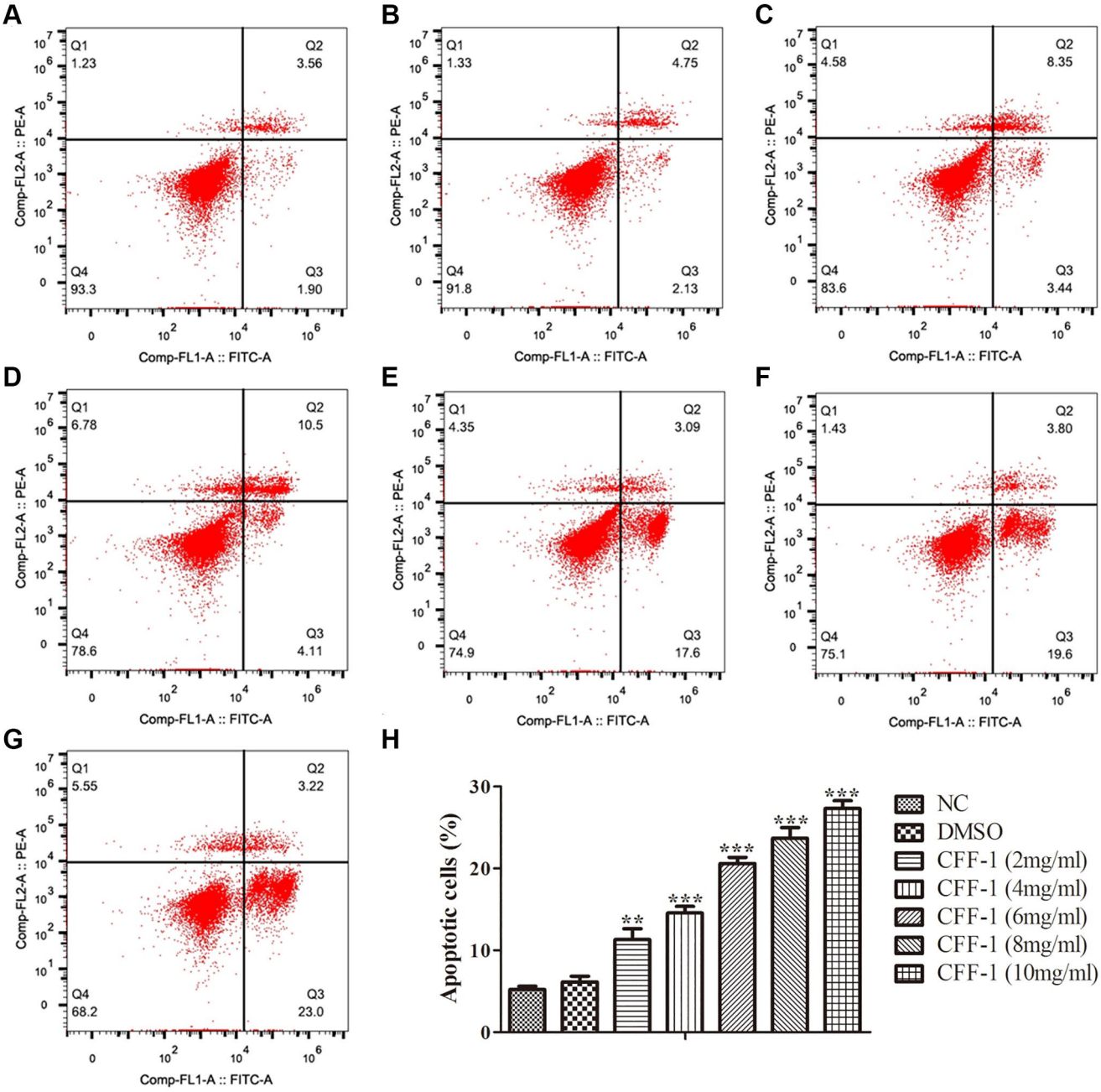

Figure 7. Apoptosis analysis of CFF-1-treated PC-3 cells by flow cytometry after 24 hours of treatment. Each panel corresponds to a different treatment condition: (**A**) NC, (**B**) DMSO, and (**C**–**G**) increasing concentrations of CFF-1 at 2, 4, 6, 8, and 10 mg/ml, respectively. (**H**) Quantitative analysis of the percentage of apoptotic cells across different treatment conditions. $^{**}p < 0.01$, $^{***}p < 0.001$.

The prognostic model we developed, anchored on these key targets, could be instrumental in tailoring personalized treatment regimens, a cornerstone of contemporary oncology. According to KEGG analysis, CFF-1 could have anti-cancer effects against PCa by regulating cancer cell proliferation and survival through PI3K-Akt, HIF-1, TNF, EGFR-TKI resistance and PD-1 checkpoint signaling pathways. This multi-pathway approach underlines the complexity and synergy of TCM in treating diseases. We carried out a series of biological function assays in diverse PCa cell lines to validate the anti-PCa ability of CFF-1. The observed inhibition of cell proliferation, migration, invasion, and induction of apoptosis in PCa cell lines are congruent with our network pharmacology predictions. This is also in line with our previous studies of PCa [11, 12].

The PI3K/Akt signaling pathway, a vital intracellular pathway, involved in tumor progression of various malignant tumors [15]. This pathway emerges as a central oncogenic axis in PCa, orchestrating a spectrum of cellular activities including proliferation, apoptosis, cell cycling, metastasis, and drug resistance [16–20]. The modulation of PI3K/Akt by CFF-1, as evidenced in our findings, could thus represent a significant stride in targeting these fundamental oncological processes. Further, our study sheds light on the role of tumor necrosis factor (TNF), predominantly produced by activated macrophages and T lymphocytes. TNF-α, the macrophage-derived variant, is known to bind to its receptor TNFR1, triggering pathways that not only elicit inflammatory responses but also induce cellular death [21, 22]. Notably, in the context of PCa, TNF-α has been implicated in promoting cell migration via the upregulation of CCR7, particularly in cases of lymph node metastasis [23]. This finding underscores the potential of targeting TNF-α as a means to impede the metastatic progression of PCa. The HIF-1 signaling pathway, another focus of our study, is critically involved in tumor pathogenesis. Activated under hypoxic conditions, this pathway is linked to tumor development, progression, and resistance to therapy, especially in PCa [24–28]. Overexpression of HIF-1α, a key component of this pathway, has been associated with poor prognoses in PCa patients [29]. Consequently, inhibiting HIF-1, as indicated by our

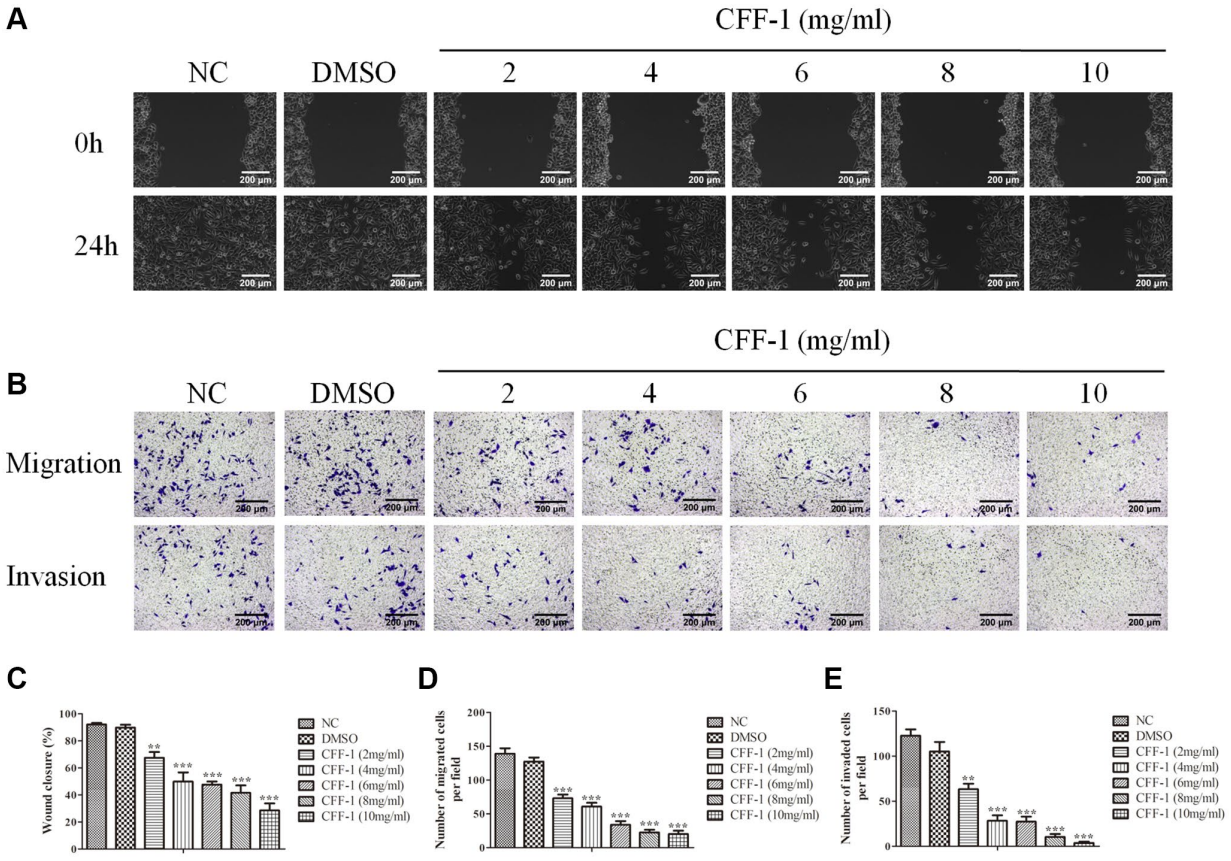

Figure 8. CFF-1 inhibited PCa cells migration and invasion. (**A**) Wound healing abilities of PC-3 cells in the presence of NC, DMSO and varying concentrations of CFF-1, with images captured at 0 and 24 hours post-wounding. (**B**) Representative images showing transwell migration and invasion assay of PC-3 cells treated with NC, DMSO and varying concentrations of CFF-1. (**C**) Quantitative analysis of the wound healing assay with different treatment conditions. (**D**) Quantitative analysis of the transwell migration assay. (**E**) Quantitative analysis of the transwell invasion assay. $^{**}p < 0.01$, $^{***}p < 0.001$.

study's results, may provide therapeutic benefits, corroborating findings from previous genetic and pharmacological studies [30–32]. IL-6, a major inflammatory factor within the tumor microenvironment, is intricately involved in tumor progression, immune modulation, and inflammatory responses [33]. Its overexpression in PCa is linked to tumor proliferation, invasion, metastasis, and the development of castration resistance [34–36]. Our research identifies IL-6 as a primary target of CFF-1, emphasizing its potential role in mitigating these malign processes. Additionally, our study delves into the realm of immune checkpoint inhibitors (ICIs), particularly targeting the PD-1/PD-L1 axis, a novel therapeutic avenue in PCa management, especially in metastatic CRPC [37]. The overexpression of PD-L1 in PCa has been correlated with poor clinical outcomes [38], highlighting the potential of ICIs in combination with other treatments as a breakthrough in PCa therapy. EGFR, a transmembrane receptor tyrosine kinase, is known for its role in activating a range of signaling pathways that contribute to tumorigenesis and progression in PCa [39–40]. Our verification of protein expression levels of key targets, including P-ERK1, NFκB1, RELA, P-mTOR, VEGFA, PD-L1, P-PI3K, P-AKT, TNF-α, P-EGFR, HIF-1α, and IL-6 in CWR22Rv1 and PC3 cell lines, reveals that CFF-1 can markedly downregulate these proteins, demonstrating

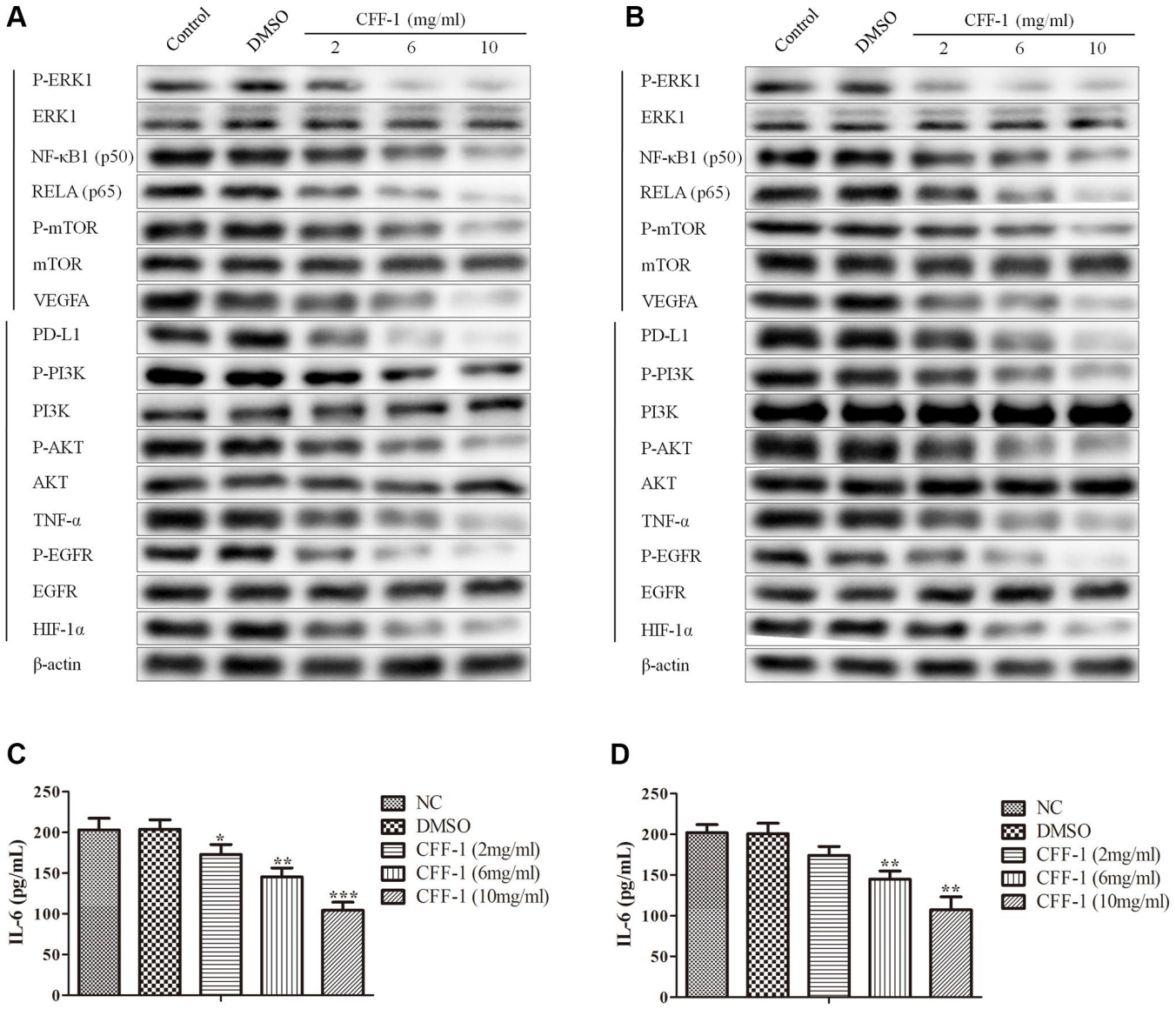

Figure 9. The relative expressions of related proteins with CFF-1 treatment on PCa cells. (**A**) The relative expressions of related proteins after 24 hours of CFF-1 treatment on PC-3 cells. (**B**) The relative expressions of related proteins after 24 hours of CFF-1 treatment on 22RV1 cells. (**C**) The secretory levels IL-6 after 48 hours of CFF-1 treatment on PC-3 cells. (**D**) The secretory levels IL-6 after 48 hours of CFF-1 treatment on 22RV1 cells.

its multifaceted therapeutic efficacy. This multi-target approach of CFF-1 suggests its potential as a comprehensive treatment option, addressing various biological processes and pathways implicated in PCa.

CONCLUSION

We demonstrated the underlying mechanism of CFF-1 against PCa based on network pharmacology and experimental evaluation. The findings may provide a strong rationale for clinical application of CFF-1 in PCa treatment.

METHODS

Screening for active ingredients of CFF-1

All ingredients of four main compounds (guizhi, fuzi, shudihuang, huangjing) in CFF-1 were acquired from TCM Systems Pharmacology Database and Analysis Platform (TCMSP, http://tcmspw.com/tcmsp.php) and a Bioinformation Analysis Tool for Molecular mechanism of Traditional Chinese Medicine (BATMAN-TCM, http://bionet.ncpsb.org/batman-tcm/). The criteria to screen for active ingredients were set as the oral bioavailability (OB) ≥30% with the drug similarity (DL) ≥0.1, and $p < 0.05$ with score >20, respectively.

Target prediction related to CFF-1 and PCa

The potential targets of active ingredients in CFF-1 were obtained from TCMSP and BATMAN-TCM. Targets related to PCa were acquired from Gene Cards database (https://www.genecards.org/) and Online Mendelian Inheritance in Man database (OMIM, http://www.omim.org/) with a keyword "prostate cancer". The UniProt database (https://www.uniprot.org/) was applied to standardize all target information, and genes without UniProt ID from human samples were eliminated. Perl software was applied to screen intersecting key targets related to both CFF-1 and PCa.

Protein–protein interaction analysis and network construction

STRING database (https://string-db.org/) is used to construct the relationship between multiple proteins. We put the key targets of CFF-1 and PCa into the STRING database Version 11.0, selecting the Homo sapiens for the species to perform the PPI network with Cytoscape software Version 3.9.1. Targets with interaction score ≥0.9 and degree ≥20 were regarded as core targets. In order to study the relationship among CFF-1, the core targets and PCa, main herbs, active ingredients and core targets were imported into the Cytoscape software to construct the herbs-active ingredients-target network.

Molecular docking

Molecular docking was carried out to evaluate the interaction between the top five targets, which exhibited high degree, and their respective active ingredients. Using the PubChem database, we acquired the 3D molecule structures of ingredients. The protein crystal structures of the targets were retrieved from the RCSB PDB database. The PyMOL software facilitated the removal of water molecules and the separation of ligands. For the conversion of small molecules and target proteins into pdbqt format, AutoDock Tools 1.5.6 was utilized. Molecular docking was performed using AutoDock Vina software. Visualization and analysis of the docking results were achieved using the PyMOL tool.

Enrichment analyses

The Gene Ontology (GO) analysis and Kyoto Encyclopedia of Genes and Genomes (KEGG) pathway enrichment were carried out through gene set enrichment analysis (GSEA) in R Version 3.7.0. Biological significance was defined as $p < 0.05$, and $Q < 0.05$.

Prognostic model construction based on key targets

RNA sequencing datasets and survival information for PCa were obtained from TCGA data portal. LASSO Cox regression was performed to screen genes with prognostic values from the key targets using R package "glmnet". A risk score formula for predicting prognosis was established as follows: risk score = expgene1 × βgene1 + expgene2 × βgene2 + … expgenen × βgene. Kaplan–Meier method was used to assess the prognostic significance of the risk score model on PCa by the R package "survival". Receiver operating characteristic (ROC) curve analysis was performed to explore the predictive power of risk score using the R package "timeROC".

We applied the CIBERSORT algorithm to assess the correlation between risk score and the infiltration of 22 immune cell subtypes [41]. Based on the ESTIMATE algorithm, we evaluated the relationship between risk score and immune score, stromal score and ESTIMATE score [42].

Cell culture and drug preparation

The human PCa cell lines CWR22Rv1 and PC-3 were cultured in RPMI-1640 medium, enriched with 10%

fetal calf serum (Gibco, Waltham, MA, USA) and maintained in a humidified atmosphere with 5% CO_2 at 37°C. CFF-1, a TCM herbal mixture, has been detailed in our previously published study [11]. A final concentration of 0, 2, 4, 6, 8 and 10 mg/mL of CFF-1 was used to treat cells.

Cell viability assay

PCa cell viability was detected by Cell Counting Kit-8 (CCK8) assay kit (Beyotime, Guangzhou, China) based on the manufacturer's instructions. PC-3 cells were seeded into 96-well plates at a density of 2×10^3 cells/well. Each well was measured at 450 nm for its absorbance.

EdU assay

In order to further evaluate cell proliferation ability, PC-3 cells were measured using the BeyoClick™ EdU-555 assay according to the manufacturer's protocol (Beyotime, Guangzhou, China). The signals were measured by fluorescence microscopy Olympus CKX53.

Clonogenic assay

PC-3 cells were transplanted into 6-well plates with a density of 2×10^3 cells/well and then the cells were treated with or without CFF-1 incubated for 10 days at 37°C. Cells were fixed in 4% paraformaldehyde and stained with crystal violet. The numbers of visible colonies were counted under an optical microscope.

Apoptosis assay

PC-3 cells were treated with various concentrations of CFF-1. After 24 h, apoptosis was detected by the annexin V-FITC apoptosis detection kit (cat. #640932, Biolegend, USA) adhering to the manufacturer's protocol.

Wound healing assay

PC-3 cells were added into 6-well plates and incubated until 100% confluence. After scraping in a straight line using a 200 μl pipette tip, the cells were rinsed thrice with PBS. Varying concentration of CFF-1 was administered to each well. The cell migration data were acquired with an inverted microscope Olympus IX51 at 0 and 24 h incubation and assessed using Image-Pro Plus 7.0 software.

Transwell migration and invasion assay

The transwell migration and invasion assay was performed using a transwell chamber system with an 8-μm pore polycarbonate membrane (Thermo Fisher Scientific, Waltham, MA, USA). For migration assay, 1×10^5 cells containing different concentrations of CFF-1 intervention and medium supplemented with 2% serum were plated onto 24-well chambers. For invasion assay, we diluted the Matrigel 1:4 with serum-free medium and seeded it to the upper chambers. Then, the cells were placed onto the upper chambers. Both assays were conducted as previously described [43].

Western blot

Total protein was extracted using RIPA buffer containing proteinase inhibitor (Best Biological, Jiangsu, China). Western blot was conducted as previously described [12]. The primary antibodies for P-ERK1, ERK1, NF-κB1, RELA, P-mTOR, mTOR, VEGFA, PD-L1, P-P13K, P13K, P-AKT, AKT, TNF-α, P-EGFR, EGFR and HIF-1α were purchased from Bioss (Beijing, China). Total protein level was normalized to β-actin.

ELISA

PC3 and CWR22Rv1 cells treated with different concentration of CFF-1 were cultured for 48 h. The supernatant of cell culture was collected and centrifuged at 1,000 g for 20 min. ELISA kits (Mlbio, Shanghai, China) were used to examine levels of IL-6 following the manufacture's instruction. We measured the absorbance at 450 nm with a microplate reader.

Statistical analysis

Statistical analyses of the *in vitro* PCa cell assays were conducted using SPSS 20.0 software. One-way univariate analysis of variance (ANOVA) was employed to analyze data obtained from at least three independent experiments, which are presented as the mean ± standard deviation. Statistical significance was defined as $p < 0.05$.

Availability of data and materials

All data included in this study are available by contacting the corresponding authors.

AUTHOR CONTRIBUTIONS

HBH, XZ and QYZ conceived and designed this study. XZ, YW and MXZ analyzed the data. QYJ, JW, LMS and Xin Yang helped discuss the results. YW, MXZ and YC drafted the manuscript. YW, MXZ and YC performed experiments mentioned in the study. All authors contributed to the article and approved the submitted version.

CONFLICTS OF INTEREST

The authors declare no conflicts of interest related to this study.

FUNDING

This work was supported by the National Natural Science Foundation of China (Grant Number: 81772732; 81702364), the Natural Science Foundation of Jiangsu Province (Grant Number: BK20171085), the Science and Technology Development Fund project of Nanjing Medical University (Grant Number: NMUB20220003), and BOXI Natural Science Cultivation Foundation of the First Affiliated Hospital of Soochow University (Grant Number: BXQN202241).

REFERENCES

1. Genkinger JM, Wu K, Wang M, Albanes D, Black A, van den Brandt PA, Burke KA, Cook MB, Gapstur SM, Giles GG, Giovannucci E, Goodman GG, Goodman PJ, et al. Measures of body fatness and height in early and mid-to-late adulthood and prostate cancer: risk and mortality in The Pooling Project of Prospective Studies of Diet and Cancer. Ann Oncol. 2020; 31:103–14. https://doi.org/10.1016/j.annonc.2019.09.007 PMID:31912782

2. Berg KD, Thomsen FB, Mikkelsen MK, Ingimarsdóttir IJ, Hansen RB, Kejs AM, Brasso K. Improved survival for patients with de novo metastatic prostate cancer in the last 20 years. Eur J Cancer. 2017; 72:20–7. https://doi.org/10.1016/j.ejca.2016.11.025 PMID:28024263

3. Marra G, Valerio M, Heidegger I, Tsaur I, Mathieu R, Ceci F, Ploussard G, van den Bergh RCN, Kretschmer A, Thibault C, Ost P, Tilki D, Kasivisvanathan V, et al, and EAU-YAU Prostate Cancer Working Party. Management of Patients with Node-positive Prostate Cancer at Radical Prostatectomy and Pelvic Lymph Node Dissection: A Systematic Review. Eur Urol Oncol. 2020; 3:565–81. https://doi.org/10.1016/j.euo.2020.08.005 PMID:32933887

4. Freedland SJ, Aronson WJ. Commentary on "Integrative clinical genomics of advanced prostate cancer". Robinson D, Van Allen EM, Wu YM, Schultz N, Lonigro RJ, Mosquera JM, Montgomery B, Taplin ME, Pritchard CC, Attard G, Beltran H, Abida W, Bradley RK, Vinson J, Cao X, Vats P, Kunju LP, Hussain M, Feng FY, Tomlins SA, Cooney KA, Smith DC, Brennan C, Siddiqui J, Mehra R, Chen Y, Rathkopf DE, Morris MJ, Solomon SB, Durack JC, Reuter VE, Gopalan A, Gao J, Loda M, Lis RT, Bowden M, Balk SP, Gaviola G, Sougnez C, Gupta M, Yu EY, Mostaghel EA, Cheng HH, Mulcahy H, True LD, Plymate SR, Dvinge H, Ferraldeschi R, Flohr P, Miranda S, Zafeiriou Z, Tunariu N, Mateo J, Perez-Lopez R, Demichelis F, Robinson BD, Schiffman M, Nanus DM, Tagawa ST, Sigaras A, Eng KW, Elemento O, Sboner A, Heath EI, Scher HI, Pienta KJ, Kantoff P, de Bono JS, Rubin MA, Nelson PS, Garraway LA, Sawyers CL, Chinnaiyan AM.Cell. 21 May 2015;161(5):1215-1228. Urol Oncol. 2017; 35:535. https://doi.org/10.1016/j.urolonc.2017.05.010 PMID:28623072

5. Zhang D, Wang Z, Li J, Zhu J. Exploring the possible molecular targeting mechanism of Saussurea involucrata in the treatment of COVID-19 based on bioinformatics and network pharmacology. Comput Biol Med. 2022; 146:105549. https://doi.org/10.1016/j.compbiomed.2022.105549 PMID:35751193

6. Zhou X, Hong Y, Zhan Y. Karacoline, identified by network pharmacology, reduces degradation of the extracellular matrix in intervertebral disc degeneration via the NF-κB signaling pathway. J Pharm Anal. 2020; 10:13–22. https://doi.org/10.1016/j.jpha.2019.07.002 PMID:32123596

7. Xu HY, Zhang YQ, Liu ZM, Chen T, Lv CY, Tang SH, Zhang XB, Zhang W, Li ZY, Zhou RR, Yang HJ, Wang XJ, Huang LQ. ETCM: an encyclopaedia of traditional Chinese medicine. Nucleic Acids Res. 2019; 47:D976–82. https://doi.org/10.1093/nar/gky987 PMID:30365030

8. Li H, Liu Z, Liu L, Li W, Cao Z, Song Z, Yang Q, Lu A, Lu C, Liu Y. Vascular Protection of TPE-CA on Hyperhomocysteinemia-induced Vascular Endothelial Dysfunction through AA Metabolism Modulated CYPs Pathway. Int J Biol Sci. 2019; 15:2037–50. https://doi.org/10.7150/ijbs.35245 PMID:31592228

9. Wang N, Li P, Hu X, Yang K, Peng Y, Zhu Q, Zhang R, Gao Z, Xu H, Liu B, Chen J, Zhou X. Herb Target Prediction Based on Representation Learning of Symptom related Heterogeneous Network. Comput Struct Biotechnol J. 2019; 17:282–90. https://doi.org/10.1016/j.csbj.2019.02.002 PMID:30867892

10. Xu L, Liu Y, Wu H, Wu H, Liu X, Zhou A. Rapid identification of chemical profile in Gandou decoction by UPLC-Q-TOF-MS(E) coupled with novel informatics UNIFI platform. J Pharm Anal. 2020; 10:35–48. https://doi.org/10.1016/j.jpha.2019.05.003 PMID:32123598

11. Wu Z, Zhu Q, Yin Y, Kang D, Cao R, Tian Q, Zhang Y, Lu S, Liu P. Traditional Chinese Medicine CFF-1 induced cell growth inhibition, autophagy, and apoptosis via inhibiting EGFR-related pathways in prostate cancer. Cancer Med. 2018; 7:1546–59. https://doi.org/10.1002/cam4.1419 PMID:29533017

12. Zhang Y, Wei Y, Jiang S, Dang Y, Yang Y, Zuo W, Zhu Q, Liu P, Gao Y, Lu S. Traditional Chinese medicine CFF-1 exerts a potent anti-tumor immunity to hinder tumor growth and metastasis in prostate cancer through EGFR/JAK1/STAT3 pathway to inhibit PD-1/PD-L1 checkpoint signaling. Phytomedicine. 2022; 99:153939. https://doi.org/10.1016/j.phymed.2022.153939 PMID:35172257

13. Huang S, Mu F, Li F, Wang W, Chen H, Lei L, Ma Y, Ding Y, Wang J. A Network-Based Approach to Explore the Mechanism and Bioactive Compounds of Erzhi Pill against Metabolic Dysfunction-Associated Fatty Liver Disease. J Diabetes Res. 2020; 2020:7867245. https://doi.org/10.1155/2020/7867245 PMID:32724826

14. Wu W, Zhang Z, Li F, Deng Y, Lei M, Long H, Hou J, Wu W. A Network-Based Approach to Explore the Mechanisms of *Uncaria* Alkaloids in Treating Hypertension and Alleviating Alzheimer's Disease. Int J Mol Sci. 2020; 21:1766. https://doi.org/10.3390/ijms21051766 PMID:32143538

15. Tortorella E, Giantulli S, Sciarra A, Silvestri I. AR and PI3K/AKT in Prostate Cancer: A Tale of Two Interconnected Pathways. Int J Mol Sci. 2023; 24:2046. https://doi.org/10.3390/ijms24032046 PMID:36768370

16. Hamidi A, Song J, Thakur N, Itoh S, Marcusson A, Bergh A, Heldin CH, Landström M. TGF-β promotes PI3K-AKT signaling and prostate cancer cell migration through the TRAF6-mediated ubiquitylation of p85α. Sci Signal. 2017; 10:eaal4186. https://doi.org/10.1126/scisignal.aal4186 PMID:28676490

17. Hashemi M, Taheriazam A, Daneii P, Hassanpour A, Kakavand A, Rezaei S, Hejazi ES, Aboutalebi M, Gholamrezaie H, Saebfar H, Salimimoghadam S, Mirzaei S, Entezari M, Samarghandian S. Targeting PI3K/Akt signaling in prostate cancer therapy. J Cell Commun Signal. 2023; 17:423–43. https://doi.org/10.1007/s12079-022-00702-1 PMID:36367667

18. Li G, Kanagasabai T, Lu W, Zou MR, Zhang SM, Celada SI, Izban MG, Liu Q, Lu T, Ballard BR, Zhou X, Adunyah SE, Matusik RJ, et al. KDM5B Is Essential for the Hyperactivation of PI3K/AKT Signaling in Prostate Tumorigenesis. Cancer Res. 2020; 80:4633–43. https://doi.org/10.1158/0008-5472.CAN-20-0505 PMID:32868382

19. Won YS, Seo KI. Sanggenol L Induces Apoptosis and Cell Cycle Arrest via Activation of p53 and Suppression of PI3K/Akt/mTOR Signaling in Human Prostate Cancer Cells. Nutrients. 2020; 12:488. https://doi.org/10.3390/nu12020488 PMID:32075054

20. Yu J, Qi H, Wang Z, Zhang Z, Song E, Song W, An R. RAB3D, upregulated by aryl hydrocarbon receptor (AhR), promotes the progression of prostate cancer by activating the PI3K/AKT signaling pathway. Cell Biol Int. 2022; 46:2246–56. https://doi.org/10.1002/cbin.11910 PMID:36153645

21. Atretkhany KN, Gogoleva VS, Drutskaya MS, Nedospasov SA. Distinct modes of TNF signaling through its two receptors in health and disease. J Leukoc Biol. 2020; 107:893–905. https://doi.org/10.1002/JLB.2MR0120-510R PMID:32083339

22. Kalliolias GD, Ivashkiv LB. TNF biology, pathogenic mechanisms and emerging therapeutic strategies. Nat Rev Rheumatol. 2016; 12:49–62. https://doi.org/10.1038/nrrheum.2015.169 PMID:26656660

23. Maolake A, Izumi K, Natsagdorj A, Iwamoto H, Kadomoto S, Makino T, Naito R, Shigehara K, Kadono Y, Hiratsuka K, Wufuer G, Nastiuk KL, Mizokami A. Tumor necrosis factor-α induces prostate cancer cell migration in lymphatic metastasis through CCR7 upregulation. Cancer Sci. 2018; 109:1524–31. https://doi.org/10.1111/cas.13586 PMID:29575464

24. Cowman SJ, Koh MY. Revisiting the HIF switch in the tumor and its immune microenvironment. Trends Cancer. 2022; 8:28–42. https://doi.org/10.1016/j.trecan.2021.10.004 PMID:34743924

25. Bao L, Chen Y, Lai HT, Wu SY, Wang JE, Hatanpaa KJ, Raisanen JM, Fontenot M, Lega B, Chiang CM, Semenza GL, Wang Y, Luo W. Methylation of hypoxia-inducible factor (HIF)-1α by G9a/GLP inhibits HIF-1 transcriptional activity and cell migration. Nucleic Acids Res. 2018; 46:6576–91. https://doi.org/10.1093/nar/gky449 PMID:29860315

26. Chen Y, Zhang B, Bao L, Jin L, Yang M, Peng Y, Kumar A, Wang JE, Wang C, Zou X, Xing C, Wang Y, Luo W.

ZMYND8 acetylation mediates HIF-dependent breast cancer progression and metastasis. J Clin Invest. 2018; 128:1937–55.
https://doi.org/10.1172/JCI95089
PMID:29629903

27. Sun X, Huang Q, Peng F, Wang J, Zhao W, Guo G. Expression and Clinical Significance of HKII and HIF-1α in Grade Groups of Prostate Cancer. Front Genet. 2021; 12:680928.
https://doi.org/10.3389/fgene.2021.680928
PMID:34220956

28. Ucaryilmaz Metin C, Ozcan G. The HIF-1α as a Potent Inducer of the Hallmarks in Gastric Cancer. Cancers (Basel). 2022; 14:2711.
https://doi.org/10.3390/cancers14112711
PMID:35681691

29. Huang M, Du H, Zhang L, Che H, Liang C. The association of HIF-1α expression with clinicopathological significance in prostate cancer: a meta-analysis. Cancer Manag Res. 2018; 10:2809–16.
https://doi.org/10.2147/CMAR.S161762
PMID:30174456

30. Mazurakova A, Koklesova L, Csizmár SH, Samec M, Brockmueller A, Šudomová M, Biringer K, Kudela E, Pec M, Samuel SM, Kassayova M, Hassan STS, Smejkal K, et al. Significance of flavonoids targeting PI3K/Akt/HIF-1α signaling pathway in therapy-resistant cancer cells - A potential contribution to the predictive, preventive, and personalized medicine. J Adv Res. 2024; 55:103–18.
https://doi.org/10.1016/j.jare.2023.02.015
PMID:36871616

31. Ouyang C, Zhang J, Lei X, Xie Z, Liu X, Li Y, Huang S, Wang Z, Tang G. Advances in antitumor research of HIF-1α inhibitor YC-1 and its derivatives. Bioorg Chem. 2023; 133:106400.
https://doi.org/10.1016/j.bioorg.2023.106400
PMID:36739684

32. Ozcan G. The hypoxia-inducible factor-1α in stemness and resistance to chemotherapy in gastric cancer: Future directions for therapeutic targeting. Front Cell Dev Biol. 2023; 11:1082057.
https://doi.org/10.3389/fcell.2023.1082057
PMID:36846589

33. Rose-John S, Jenkins BJ, Garbers C, Moll JM, Scheller J. Targeting IL-6 trans-signalling: past, present and future prospects. Nat Rev Immunol. 2023; 23:666–81.
https://doi.org/10.1038/s41577-023-00856-y
PMID:37069261

34. Culig Z, Puhr M. Interleukin-6 and prostate cancer: Current developments and unsolved questions. Mol Cell Endocrinol. 2018; 462:25–30.
https://doi.org/10.1016/j.mce.2017.03.012
PMID:28315704

35. Yamaguchi M, Hashimoto K, Jijiwa M, Murata T. The inflammatory macrophages repress the growth of bone metastatic human prostate cancer cells via TNF-α and IL-6 signaling: Involvement of cell signaling regulator regucalcin. Cell Signal. 2023; 107:110663.
https://doi.org/10.1016/j.cellsig.2023.110663
PMID:37001596

36. Yang F, Yuan C, Wu D, Zhang J, Zhou X. IRE1α Expedites the Progression of Castration-Resistant Prostate Cancers *via* the Positive Feedback Loop of IRE1α/IL-6/AR. Front Oncol. 2021; 11:671141.
https://doi.org/10.3389/fonc.2021.671141
PMID:34295814

37. Xu Y, Song G, Xie S, Jiang W, Chen X, Chu M, Hu X, Wang ZW. The roles of PD-1/PD-L1 in the prognosis and immunotherapy of prostate cancer. Mol Ther. 2021; 29:1958–69.
https://doi.org/10.1016/j.ymthe.2021.04.029
PMID:33932597

38. Gevensleben H, Dietrich D, Golletz C, Steiner S, Jung M, Thiesler T, Majores M, Stein J, Uhl B, Müller S, Ellinger J, Stephan C, Jung K, et al. The Immune Checkpoint Regulator PD-L1 Is Highly Expressed in Aggressive Primary Prostate Cancer. Clin Cancer Res. 2016; 22:1969–77.
https://doi.org/10.1158/1078-0432.CCR-15-2042
PMID:26573597

39. Shostak K, Chariot A. EGFR and NF-κB: partners in cancer. Trends Mol Med. 2015; 21:385–93.
https://doi.org/10.1016/j.molmed.2015.04.001
PMID:25979753

40. Liao Y, Guo Z, Xia X, Liu Y, Huang C, Jiang L, Wang X, Liu J, Huang H. Inhibition of EGFR signaling with Spautin-1 represents a novel therapeutics for prostate cancer. J Exp Clin Cancer Res. 2019; 38:157.
https://doi.org/10.1186/s13046-019-1165-4
PMID:30975171

41. Newman AM, Liu CL, Green MR, Gentles AJ, Feng W, Xu Y, Hoang CD, Diehn M, Alizadeh AA. Robust enumeration of cell subsets from tissue expression profiles. Nat Methods. 2015; 12:453–7.
https://doi.org/10.1038/nmeth.3337
PMID:25822800

42. Yoshihara K, Shahmoradgoli M, Martínez E, Vegesna R, Kim H, Torres-Garcia W, Treviño V, Shen H, Laird PW, Levine DA, Carter SL, Getz G, Stemke-Hale K, et al. Inferring tumour purity and stromal and immune cell admixture from expression data. Nat Commun. 2013; 4:2612.

https://doi.org/10.1038/ncomms3612
PMID:24113773

43. Wei G, Yang X, Lu H, Zhang L, Wei Y, Li H, Zhu M, Zhou X. Prognostic value and immunological role of FOXM1 in human solid tumors. Aging (Albany NY). 2022; 14:9128–48.
https://doi.org/10.18632/aging.204394
PMID:36435510

SUPPLEMENTARY MATERIALS

Supplementary Figures

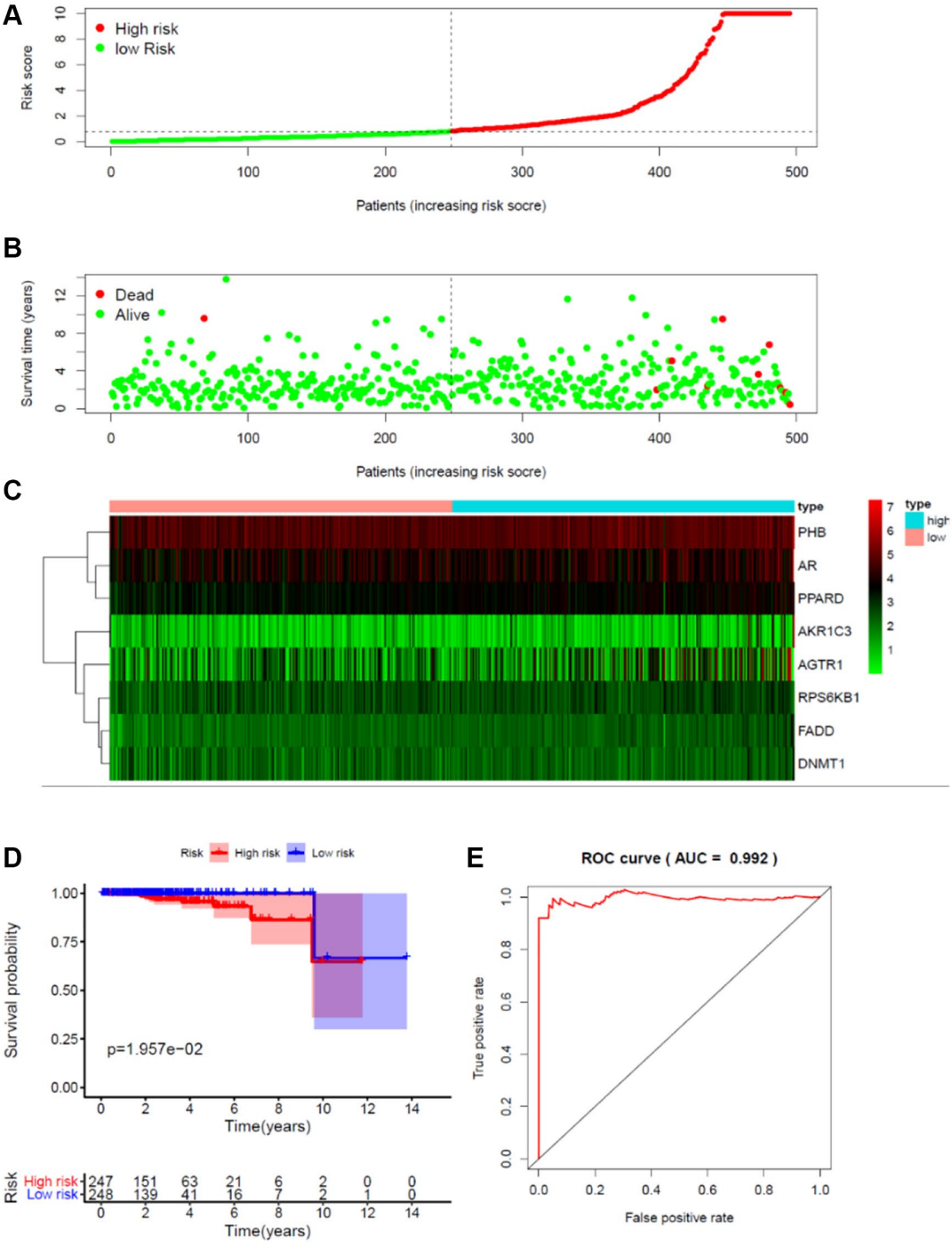

Supplementary Figure 1. Risk score for target gene signature and OS in PCa patients. (**A**) Risk score of an 8-gene signature for predicting OS. (**B**) Survival status and duration of cases. (**C**) Heatmap of the 8 gene expression in PCa patients. (**D**) Kaplan-Meier curve for OS in the low- and high-risk groups. (**E**) ROC curve for the OS prediction of risk score model.

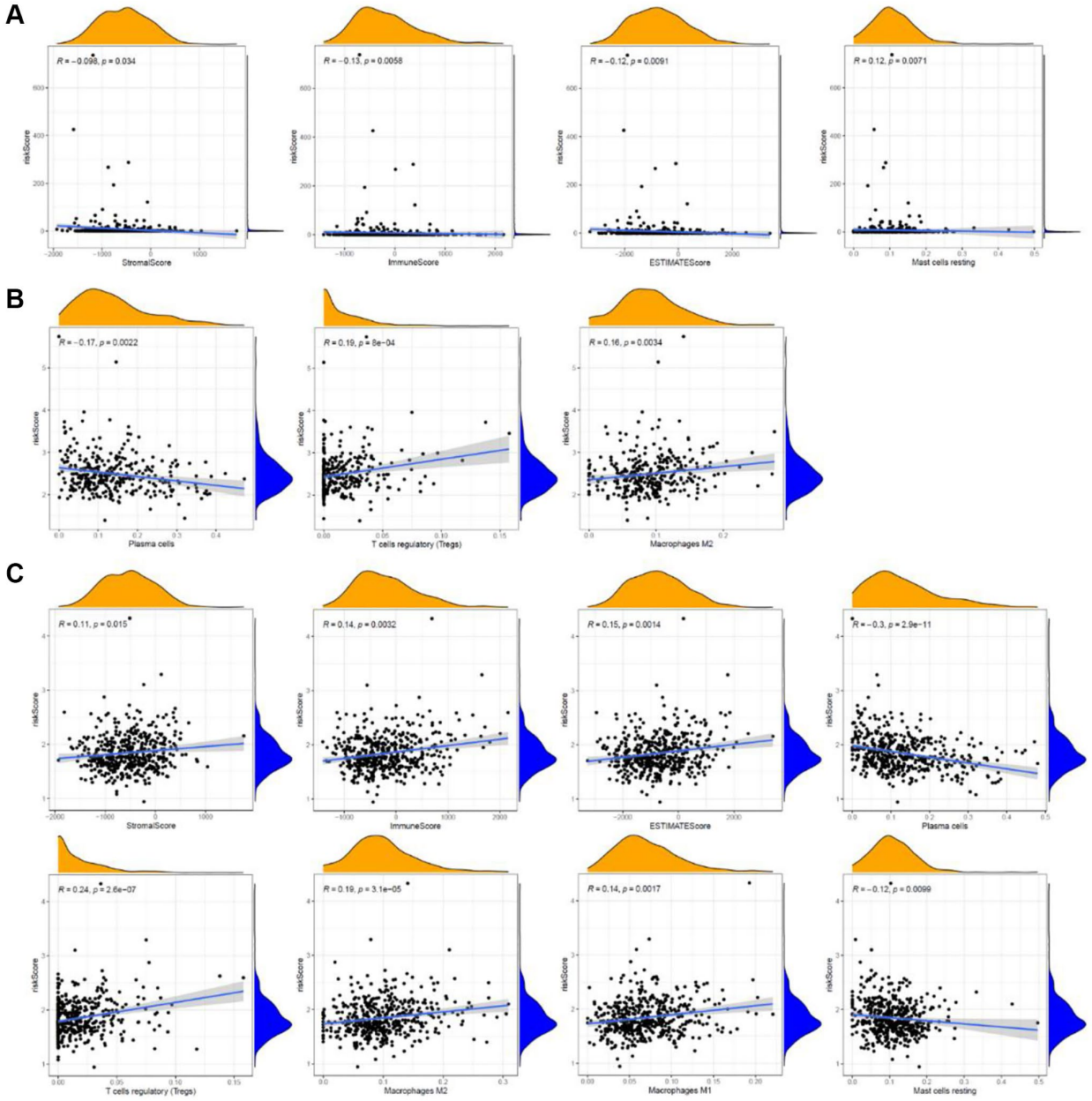

Supplementary Figure 2. The significant associations of the risk scores with immune score, stromal score, ESTIMATE score, and the infiltration of 22 immune cell subtypes. (**A**) The associations of risk score for predicting OS of PCa patients with immune score, stromal score, ESTIMATE score, and the infiltration of immune cell subtypes. (**B**) The associations of risk score for predicting DFS of PCa patients with the infiltration of immune cell subtypes. (**C**) The associations of risk score for predicting PFS of PCa patients with immune score, stromal score, ESTIMATE score, and the infiltration of 22 immune cell subtypes.

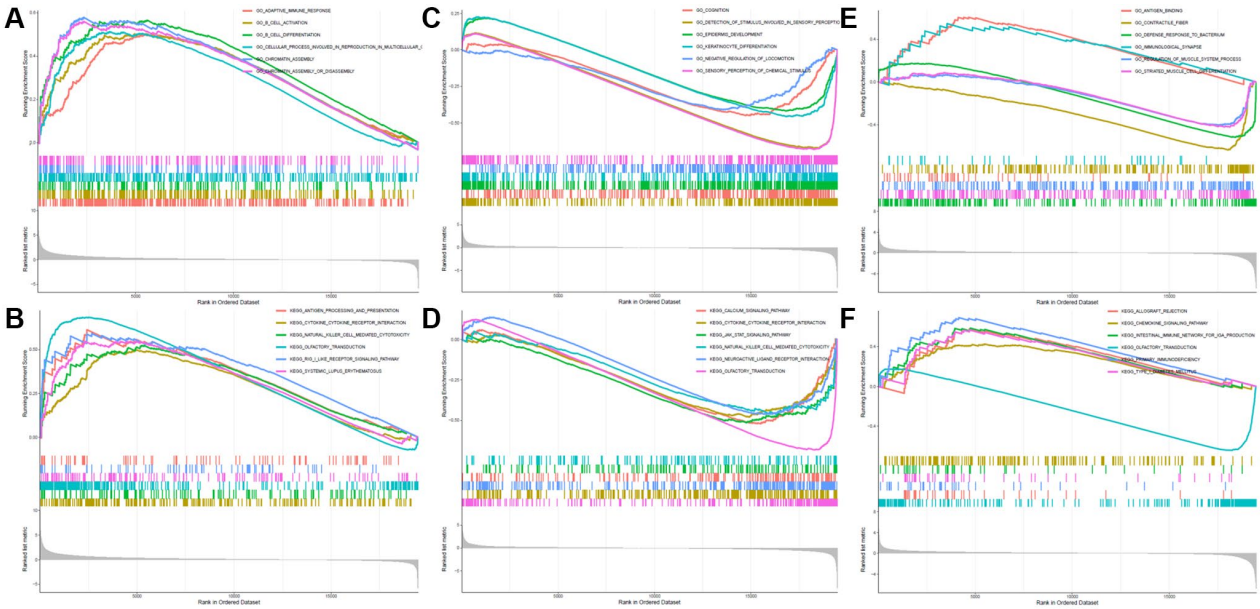

Supplementary Figure 3. (**A**, **B**) DNMT3B correlation with signaling pathways in GO (**A**) and KEGG (**B**) collection. (**C**, **D**) HPRT1 correlation with signaling pathways in GO (**C**) and KEGG (**D**) collection. (**E**, **F**) RXRB correlation with signaling pathways in GO (**E**) and KEGG (**F**) collection.

Supplementary Tables

Supplementary Table 1. KEGG pathway analysis of 359 key targets.

Pathway	*p*-value	Pathway	*p*-value	Pathway	*p*-value
Lipid and atherosclerosis	3.72E-25	Fluid shear stress and atherosclerosis	1.38E-22	Chagas disease	9.58E-22
AGE-RAGE signaling pathway in diabetic complications	6.00E-20	HIF-1 signaling pathway	8.91E-20	Prostate cancer	1.73E-19
Proteoglycans in cancer	8.59E-19	Hepatitis B	1.68E-18	Human cytomegalovirus infection	4.75E-18
Non-alcoholic fatty liver disease	5.33E-18	Thyroid hormone signaling pathway	1.71E-17	TNF signaling pathway	1.19E-16
Th17 cell differentiation	2.61E-16	Colorectal cancer	4.38E-16	EGFR tyrosine kinase inhibitor resistance	4.38E-16
IL-17 signaling pathway	4.61E-16	PI3K-Akt signaling pathway	8.65E-16	Gastric cancer	1.27E-15
Kaposi sarcoma-associated herpesvirus infection	3.27E-15	African trypanosomiasis	8.33E-15	Endocrine resistance	1.19E-14
Breast cancer	3.77E-14	Pancreatic cancer	1.68E-13	Hepatitis C	2.51E-13
Human immunodeficiency virus 1 infection	3.59E-13	Tuberculosis	3.67E-13	Toll-like receptor signaling pathway	4.16E-13
Influenza A	5.20E-13	Acute myeloid leukemia	8.91E-13	Toxoplasmosis	2.49E-12
PD-L1 expression and PD-1 checkpoint pathway in cancer	5.28E-12	MAPK signaling pathway	5.81E-12	Apoptosis	6.46E-12
Insulin resistance	6.90E-12	Osteoclast differentiation	8.63E-12	Measles	1.05E-11
Human papillomavirus infection	1.73E-11	Prolactin signaling pathway	1.88E-11	C-type lectin receptor signaling pathway	1.88E-11
Antifolate resistance	2.88E-11	Inflammatory bowel disease	4.00E-11	Platinum drug resistance	4.06E-11
Human T-cell leukemia virus 1 infection	7.71E-11	T cell receptor signaling pathway	1.24E-10	Parathyroid hormone synthesis, secretion and action	1.82E-10
Hepatocellular carcinoma	1.82E-10	Diabetic cardiomyopathy	1.96E-10	Yersinia infection	2.13E-10
Pathogenic Escherichia coli infection	4.06E-10	ErbB signaling pathway	7.10E-10	Leishmaniasis	8.45E-10
Adipocytokine signaling pathway	9.24E-10	Renal cell carcinoma	9.24E-10	Non-small cell lung cancer	1.95E-09
FoxO signaling pathway	2.33E-09	Small cell lung cancer	2.90E-09	Amoebiasis	3.03E-09
Epstein-Barr virus infection	3.03E-09	MicroRNAs in cancer	4.35E-09	Estrogen signaling pathway	6.48E-09
Neurotrophin signaling pathway	9.59E-09	Type II diabetes mellitus	9.61E-09	mTOR signaling pathway	1.41E-08
Alzheimer disease	1.63E-08	Shigellosis	2.14E-08	Endometrial cancer	2.91E-08
VEGF signaling pathway	3.70E-08	Relaxin signaling pathway	4.14E-08	AMPK signaling pathway	5.55E-08
Ras signaling pathway	7.09E-08	Th1 and Th2 cell differentiation	9.93E-08	NF-kappa B signaling pathway	1.29E-07
Focal adhesion	1.63E-07	Pertussis	1.93E-07	Chronic myeloid leukemia	1.93E-07
Sphingolipid signaling pathway	2.28E-07	Coronavirus disease - COVID-19	2.39E-07	Malaria	2.39E-07
Choline metabolism in cancer	2.47E-07	Fc epsilon RI signaling pathway	2.47E-07	Pathways of neurodegeneration - multiple diseases	2.97E-07
Longevity regulating pathway	3.04E-07	Salmonella infection	3.04E-07	Central carbon metabolism in cancer	3.54E-07
Aldosterone-regulated sodium reabsorption	5.05E-07	Thyroid cancer	5.05E-07	Melanoma	5.07E-07
B cell receptor signaling pathway	5.07E-07	Glioma	8.77E-07	Inflammatory mediator regulation of TRP channels	1.21E-06
Rap1 signaling pathway	1.22E-06	cAMP signaling pathway	2.10E-06	Chemokine signaling pathway	2.82E-06
Transcriptional misregulation in cancer	2.82E-06	Rheumatoid arthritis	2.84E-06	Longevity regulating pathway - multiple species	2.91E-06

Oxytocin signaling pathway	3.20E-06	TGF-beta signaling pathway	3.20E-06	Signaling pathways regulating pluripotency of stem cells	3.79E-06
Hippo signaling pathway	4.28E-06	Phospholipase D signaling pathway	6.43E-06	Insulin signaling pathway	7.72E-06
Apoptosis - multiple species	9.85E-06	Cellular senescence	1.42E-05	Basal cell carcinoma	2.02E-05
GnRH secretion	2.37E-05	Viral carcinogenesis	2.45E-05	JAK-STAT signaling pathway	2.45E-05
PPAR signaling pathway	2.80E-05	Platelet activation	2.82E-05	Cholinergic synapse	3.35E-05
NOD-like receptor signaling pathway	3.74E-05	Regulation of lipolysis in adipocytes	3.97E-05	Allograft rejection	4.16E-05
Cushing syndrome	4.27E-05	Natural killer cell mediated cytotoxicity	5.59E-05	Necroptosis	6.05E-05
Adherens junction	6.42E-05	Vascular smooth muscle contraction	6.65E-05	Bladder cancer	7.62E-05
Ovarian steroidogenesis	7.83E-05	Type I diabetes mellitus	0.000112	Progesterone-mediated oocyte maturation	0.00012
Regulation of actin cytoskeleton	0.000185	Legionellosis	0.000206	Neutrophil extracellular trap formation	0.000215
Growth hormone synthesis, secretion and action	0.000217	Calcium signaling pathway	0.000274	Prion disease	0.000288
Autophagy - animal	0.000313	Fc gamma R-mediated phagocytosis	0.000328	cGMP-PKG signaling pathway	0.000339
p53 signaling pathway	0.000362	Leukocyte transendothelial migration	0.000463	Melanogenesis	0.00048
Graft-versus-host disease	0.000534	Dopaminergic synapse	0.000646	GnRH signaling pathway	0.000796
Cytokine-cytokine receptor interaction	0.000886	Renin secretion	0.000936	RIG-I-like receptor signaling pathway	0.001046
Adrenergic signaling in cardiomyocytes	0.002414	Wnt signaling pathway	0.002467	Neuroactive ligand-receptor interaction	0.003181
Arginine biosynthesis	0.003267	Epithelial cell signaling in Helicobacter pylori infection	0.004089	Herpes simplex virus 1 infection	0.004216
Serotonergic synapse	0.004913	Viral myocarditis	0.005566	Gap junction	0.005838
Axon guidance	0.006027	Steroid hormone biosynthesis	0.006061	Intestinal immune network for IgA production	0.006578
Cocaine addiction	0.006578	Hypertrophic cardiomyopathy	0.006663	Cholesterol metabolism	0.007292
Autoimmune thyroid disease	0.010071	Retinol metabolism	0.011432	Amphetamine addiction	0.012406
Asthma	0.014127	Insulin secretion	0.014819	Tight junction	0.016568
Long-term depression	0.019059	Bile secretion	0.019386	Biosynthesis of amino acids	0.019535
Carbohydrate digestion and absorption	0.020249	Arachidonic acid metabolism	0.020299	Bacterial invasion of epithelial cells	0.022309
Cytosolic DNA-sensing pathway	0.023738	Tyrosine metabolism	0.024982	Oocyte meiosis	0.027646
Apelin signaling pathway	0.041067				

Supplementary Table 2. GO process analysis of 359 key targets.

Pathway	*p*-value	Pathway	*p*-value	Pathway	*p*-value
nuclear receptor activity	8.09E-21	transcription factor activity, direct ligand regulated sequence-specific DNA binding	8.09E-21	steroid hormone receptor activity	1.07E-20
receptor ligand activity	2.30E-20	receptor regulator activity	5.25E-20	cytokine receptor binding	2.70E-16
protein heterodimerization activity	9.69E-16	cofactor binding	1.06E-15	proximal promoter sequence-specific DNA binding	1.60E-14
RNA polymerase II proximal promoter sequence-specific DNA binding	1.60E-14	steroid binding	4.04E-14	chromatin binding	1.07E-13
cytokine activity	1.58E-13	heme binding	5.32E-11	hormone binding	5.33E-11
carboxylic acid binding	1.87E-10	phosphatase binding	1.98E-10	organic acid binding	2.09E-10
tetrapyrrole binding	2.09E-10	growth factor activity	2.30E-10	growth factor receptor binding	4.09E-10
hormone receptor binding	4.89E-10	coenzyme binding	1.01E-08	nuclear hormone receptor binding	1.14E-08
ubiquitin-like protein ligase binding	1.79E-08	oxidoreductase activity, acting on paired donors, with incorporation or reduction of molecular oxygen	2.35E-08	ubiquitin protein ligase binding	2.44E-08
vitamin binding	5.45E-08	monocarboxylic acid binding	8.89E-08	DNA-binding transcription activator activity, RNA polymerase II-specific	1.56E-07
NADP binding	1.56E-07	G protein-coupled receptor binding	4.22E-07	protein phosphatase binding	5.23E-07
tau protein binding	6.14E-07	transcription coregulator activity	6.14E-07	histone deacetylase binding	7.36E-07
protease binding	9.45E-07	nuclear receptor binding	9.59E-07	oxidoreductase activity, acting on the CH-CH group of donors	1.29E-06
phosphoprotein binding	1.29E-06	enzyme activator activity	2.02E-06	chemoattractant activity	2.02E-06
antioxidant activity	2.02E-06	estrogen receptor binding	2.70E-06	histone kinase activity	3.83E-06
monooxygenase activity	4.54E-06	amide binding	4.85E-06	steroid hormone receptor binding	5.53E-06
scaffold protein binding	5.53E-06	tumor necrosis factor receptor superfamily binding	5.53E-06	insulin-like growth factor receptor binding	5.53E-06
iron ion binding	6.67E-06	protein serine/threonine kinase activity	6.67E-06	E-box binding	1.11E-05
oxidoreductase activity, acting on the CH-CH group of donors, NAD or NADP as acceptor	1.14E-05	RNA polymerase II transcription factor binding	1.14E-05	integrin binding	1.14E-05
death receptor binding	1.14E-05	adrenergic receptor binding	1.14E-05	transcription coactivator activity	1.18E-05
kinase regulator activity	1.37E-05	protein serine/threonine/tyrosine kinase activity	2.01E-05	enhancer binding	2.28E-05
heat shock protein binding	3.90E-05	protein phosphorylated amino acid binding	4.11E-05	transcription coactivator binding	4.15E-05
oxidoreductase activity, acting on paired donors, with incorporation or reduction of molecular oxygen, NAD(P)H as one donor, and incorporation of one atom of oxygen	5.53E-05	electron transfer activity	7.64E-05	ammonium ion binding	7.64E-05
neurotransmitter binding	8.02E-05	protein tyrosine kinase activity	0.000105456	alcohol dehydrogenase (NADP+) activity	0.000108
NADPH binding	0.00010771	hormone activity	0.000125943	transcription cofactor binding	0.000133
oxygen binding	0.000176291	oxidoreductase activity, acting on the CH-OH group of donors, NAD or NADP as acceptor	0.00019025	fatty acid binding	0.000215
kinase activator activity	0.000254366	tumor necrosis factor receptor binding	0.000318127	insulin receptor substrate binding	0.000344
cholesterol transporter activity	0.00034585	disordered domain specific binding	0.00037338	insulin receptor binding	0.000442
oxidoreductase activity, acting on CH-OH group of donors	0.000460999	growth factor binding	0.000491722	activating transcription factor binding	0.000527
peptide binding	0.000532798	tau-protein kinase activity	0.00053822	oxidoreductase activity, acting on the aldehyde or oxo group of donors, NAD or NADP as acceptor	0.000596
dioxygenase activity	0.000661983	sterol transporter activity	0.000661983	flavin adenine dinucleotide binding	0.00068
sulfur compound binding	0.000680429	protein kinase activator activity	0.000748104	cysteine-type endopeptidase regulator activity involved in apoptotic process	0.00078
aldo-keto reductase (NADP) activity	0.000788194	phosphotyrosine residue binding	0.000895584	protein kinase A catalytic subunit binding	0.00091
retinoic acid receptor binding	0.000948814	Hsp90 protein binding	0.001013403	SMAD binding	0.001047
FAD binding	0.001131296	oxidoreductase activity, acting on the aldehyde or oxo group of donors	0.001142252	protein kinase regulator activity	0.001148
translation repressor activity, mRNA regulatory element binding	0.001148329	platelet-derived growth factor receptor binding	0.001148329	long-chain fatty acid binding	0.001148
protein self-association	0.001206353	oxidoreductase activity, acting on peroxide as acceptor	0.00124775	protein C-terminus binding	0.001257
retinoid X receptor binding	0.001484449	chromatin DNA binding	0.001513989	cholesterol binding	0.001578
cell adhesion molecule binding	0.001577986	repressing transcription factor binding	0.001577986	beta-catenin binding	0.001599

peptidase regulator activity	0.001614389	extracellular matrix binding	0.001735213	protein kinase C activity	0.001801
receptor serine/threonine kinase binding	0.001801096	NF-kappaB binding	0.001989279	heparin binding	0.002056
lipid transporter activity	0.002128739	nuclear receptor transcription coactivator activity	0.002128739	glycosaminoglycan binding	0.002137
modified amino acid binding	0.002634546	sterol binding	0.002643398	enhancer sequence-specific DNA binding	0.002716
transmembrane receptor protein tyrosine kinase activity	0.003269562	steroid hydroxylase activity	0.00336663	transforming growth factor beta receptor binding	0.004106
serine hydrolase activity	0.00427316	alcohol binding	0.00427316	fibroblast growth factor binding	0.00484
translation regulator activity, nucleic acid binding	0.004840122	peptidase activator activity	0.004971609	insulin-like growth factor I binding	0.00524
Toll-like receptor binding	0.005240093	NADP-retinol dehydrogenase activity	0.005240093	transmembrane receptor protein serine/threonine kinase binding	0.00524
RNA polymerase II activating transcription factor binding	0.005373752	peroxidase activity	0.005373752	non-membrane spanning protein tyrosine kinase activity	0.005374
mitogen-activated protein kinase binding	0.005455186	DNA-binding transcription repressor activity, RNA polymerase II-specific	0.005567454	oxidoreductase activity, acting on single donors with incorporation of molecular oxygen, incorporation of two atoms of oxygen	0.006361
translation repressor activity	0.006361033	folic acid binding	0.006577534	protein kinase B binding	0.006578
platelet-derived growth factor binding	0.006577534	I-SMAD binding	0.006577534	fibronectin binding	0.007213
oxidoreductase activity, acting on single donors with incorporation of molecular oxygen	0.007212618	transcription corepressor activity	0.007460244	catalytic activity, acting on DNA	0.007549
Hsp70 protein binding	0.007899398	interleukin-1 receptor binding	0.008250906	catecholamine binding	0.008251
voltage-gated cation channel activity	0.008952296	lipoprotein particle receptor binding	0.009383432	serine-type peptidase activity	0.009677
enzyme inhibitor activity	0.009974901	serine-type endopeptidase activity	0.009974901	MAP kinase kinase activity	0.010172
androgen receptor binding	0.010272915	G protein-coupled amine receptor activity	0.010318019	bHLH transcription factor binding	0.010318
protein serine/threonine kinase activator activity	0.010318019	neurotransmitter receptor activity	0.010348568	RNA polymerase II distal enhancer sequence-specific DNA binding	0.010897
transmembrane receptor protein kinase activity	0.01089714	protein kinase A binding	0.01089714	protein kinase C binding	0.011877
promoter-specific chromatin binding	0.011876902	retinol dehydrogenase activity	0.011945223	actinin binding	0.012818
protein phosphatase 2A binding	0.012817505	cation channel activity	0.013691175	translation regulator activity	0.013929
opsonin binding	0.014210904	lipase inhibitor activity	0.014210904	steroid dehydrogenase activity	0.015944
amyloid-beta binding	0.015944247	cysteine-type endopeptidase activator activity involved in apoptotic process	0.01666463	chloride channel regulator activity	0.016665
MHC class II protein complex binding	0.01666463	apolipoprotein binding	0.01666463	oxidoreductase activity, acting on NAD(P)H	0.017216
virus receptor activity	0.018832345	hijacked molecular function	0.018832345	ion gated channel activity	0.019364
DNA polymerase binding	0.019400305	gated channel activity	0.019649029	cysteine-type endopeptidase inhibitor activity	0.019649
copper ion binding	0.019649029	cytokine binding	0.02057876	lipoprotein particle binding	0.020579
protein-lipid complex binding	0.02057876	channel regulator activity	0.021625653	ATPase binding	0.021712
RNA polymerase II basal transcription factor binding	0.021784633	cyclin-dependent protein serine/threonine kinase regulator activity	0.021784633	retinoid binding	0.022287
channel activity	0.022469788	passive transmembrane transporter activity	0.022923969	cysteine-type endopeptidase activity	0.023506
isoprenoid binding	0.02412412	voltage-gated ion channel activity	0.02412412	voltage-gated channel activity	0.024124
peptidase activator activity involved in apoptotic process	0.024380968	cysteine-type endopeptidase inhibitor activity involved in apoptotic process	0.024380968	protein tyrosine kinase binding	0.024618
voltage-gated calcium channel activity	0.025914078	receptor tyrosine kinase binding	0.026221153	L-ascorbic acid binding	0.02771
protein N-terminus binding	0.029624628	RNA polymerase II core promoter sequence-specific DNA binding	0.031383956	neuropeptide hormone activity	0.031384
collagen binding	0.031583969	endopeptidase activity	0.032267629	oxidoreductase activity, acting on paired donors, with incorporation or reduction of molecular oxygen, 2-oxoglutarate as one donor, and incorporation of one atom each of oxygen into both donors	0.032873
lyase activity	0.03316175	double-stranded RNA binding	0.03316175	phospholipid binding	0.03808
calcium channel activity	0.03807999	core promoter binding	0.03807999	ion channel binding	0.038386
mRNA 5′-UTR binding	0.038386203	R-SMAD binding	0.038386203	fatty acid derivative binding	0.038386
p53 binding	0.038802999	chaperone binding	0.041073421	pyridoxal phosphate binding	0.043332
endopeptidase inhibitor activity	0.045706496	vitamin B6 binding	0.046377378	fibroblast growth factor receptor binding	0.046883
MHC protein complex binding	0.046883431				